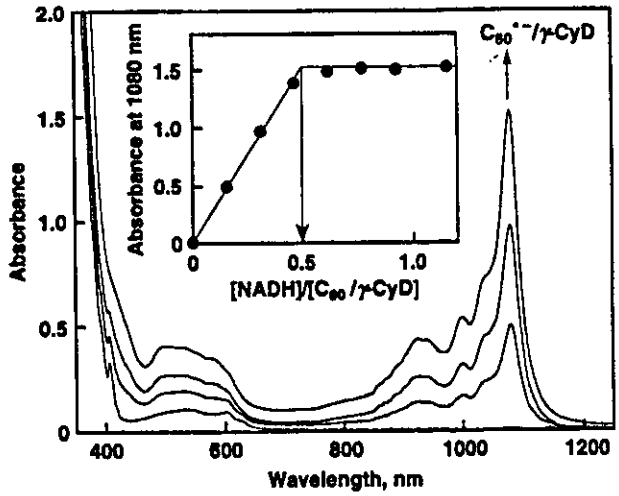

Figure 3. Vis-NIR spectra of deaerated phosphate buffer (50 mM, pH 7.4) of C_{60}/γ-CyD (1.3×10^{-4} M) with NADH (0, 2.0×10^{-5}, 4.0×10^{-5}, 1.5×10^{-4} M) after visible-light irradiation with a Xe lamp ($\lambda > 470$ nm) for 2 h at 298 K. Inset: Plot of the absorbance at 1080 nm vs [NADH]/[C_{60}/γ-CyD].

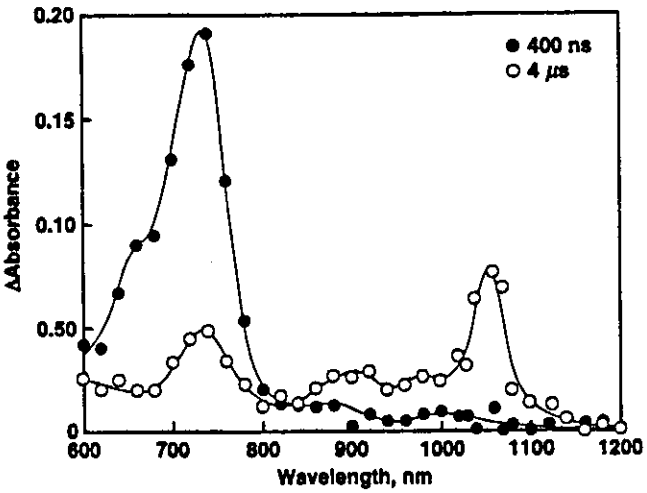

Figure 4. Transient absorption spectra observed in the photoreduction of C_{60}/γ-CyD (5.5×10^{-5} M) by NADH (4.0×10^{-3} M) at 400 ns and 4 μs after laser excitation in deaerated phosphate buffer (50 mM, pH 7.4) at 295 K.

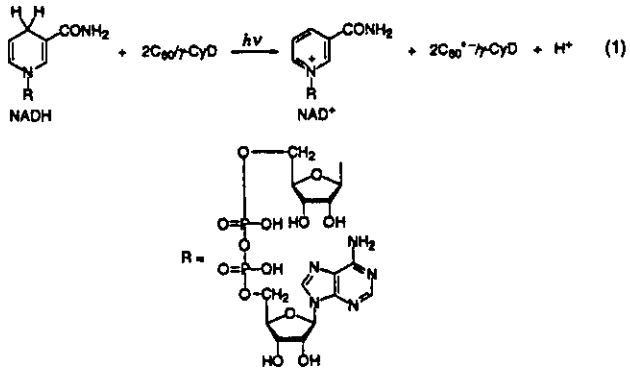

The singlet excited state of C_{60} produced initially upon irradiation is known to be efficiently converted to the triplet excited state by the fast intersystem crossing.[12,13] The transient absorption spectra in the visible and NIR region are observed by the laser flash photolysis of a deaerated aqueous solution of C_{60}/γ-CyD in the presence of NADH with 532 nm laser light as shown in Figure 4.

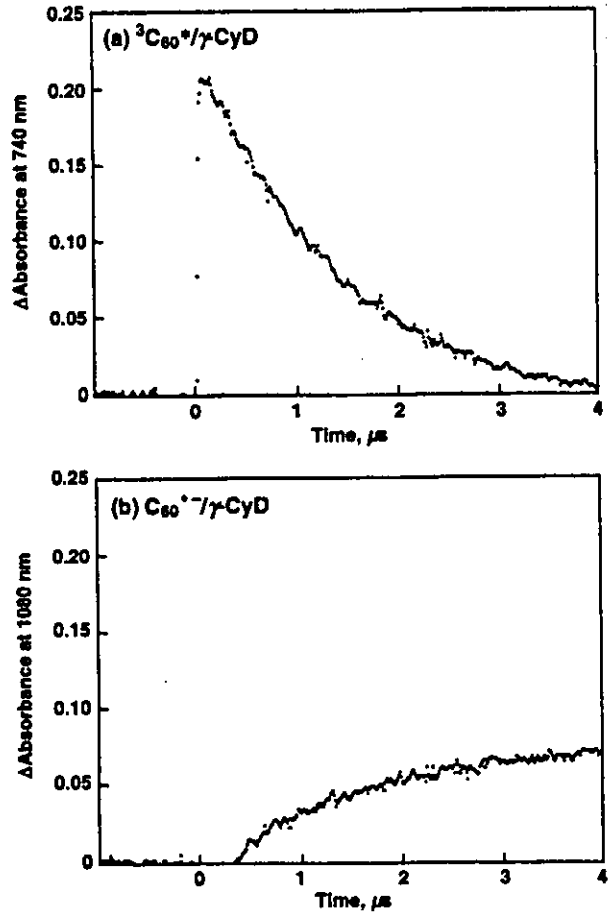

Figure 5. (a) Decay of the absorbance at 740 nm due to $^3C_{60}$*/γ-CyD and (b) rise of the absorbance at 1080 nm due to $C_{60}^{\bullet-}$/γ-CyD observed in the photoreduction of C_{60}/γ-CyD (5.5×10^{-5} M) by NADH (8.0×10^{-3} M) after laser excitation in deaerated phosphate buffer (50 mM, pH 7.4) at 295 K.

SCHEME 2

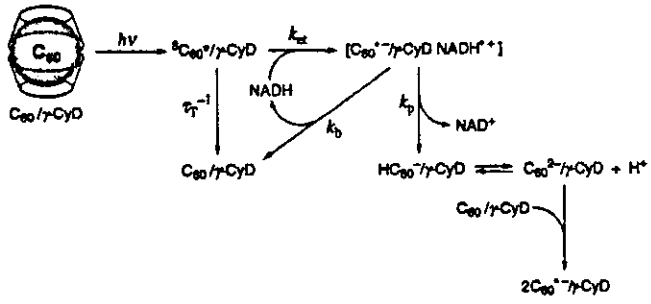

The transient absorption band at 740 nm appearing immediately after nanosecond laser pulse excitation is attributed to the triplet–triplet absorption band of $^3C_{60}$*/γ-CyD. The decay of the absorption band of $^3C_{60}$*/γ-CyD is accompanied by appearance of a new absorption band at 1080 nm which is diagnostic of $C_{60}^{\bullet-}$/γ-CyD. The decay of the absorbance at 740 nm due to $^3C_{60}$*/γ-CyD obeys pseudo-first-order kinetics, coinciding with the rise of the absorbance at 1080 nm due to $C_{60}^{\bullet-}$/γ-CyD as shown in Figure 5.

The mechanism for generation of two equivalents of $C_{60}^{\bullet-}$/γ-CyD in eq 1 may be essentially the same as reported for the photoreduction of C_{60} by an NADH model compound,[38] as shown in Scheme 2. First photoinduced electron transfer from NADH to $^3C_{60}$*/γ-CyD (k_{et}) occurs to give the radical ion pair [$C_{60}^{\bullet-}$/γ-CyD NADH$^{\bullet+}$] in competition with the decay of $^3C_{60}$*/

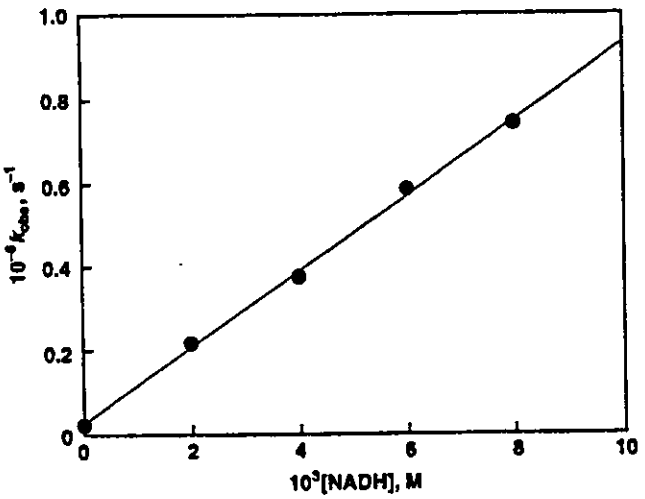

Figure 6. Plots of k_{obs} vs [NADH] in the photoreduction of C_{60}/γ-CyD (5.5×10^{-5} M) by [NADH] in deaerated phosphate buffer (50 mM, pH 7.4) at 298 K.

γ-CyD to the ground state (τ_T^{-1}). This is followed a hydrogen (or proton and electron) transfer from $NADH^{\bullet+}$ to $C_{60}^{\bullet-}$/γ-CyD (k_p) to produce HC_{60}^-/γ-CyD and NAD^+ in competition with the back electron transfer to the reactant pair (k_b), The subsequent facile electron transfer from C_{60}^{2-}/γ-CyD being in equilibrium with HC_{60}^-/γ-CyD to C_{60}/γ-CyD leads to formation of two equivalents of $C_{60}^{\bullet-}$/γ-CyD (Scheme 2)

According to Scheme 2, the decay of $^3C_{60}$*/γ-CyD and the concomitant appearance of $C_{60}^{\bullet-}$/γ-CyD are derived as given by eqs 2 and 3, respectively

$$[^3C_{60}\text{*}/\gamma\text{-CyD}] = [^3C_{60}\text{*}/\gamma\text{-CyD}]_0 \exp[-(k_{et}[\text{NADH}] + \tau_T^{-1})t] \quad (2)$$

$$[C_{60}^{\bullet-}/\gamma\text{-CyD}] = [C_{60}^{\bullet-}/\gamma\text{-CyD}]_\infty (1 - \exp[-(k_{et}[\text{NADH}] + \tau_T^{-1})t]) \quad (3)$$

In eq 3, $[C_{60}^{\bullet-}/\gamma\text{-CyD}]_\infty$ is the concentration of $C_{60}^{\bullet-}$/γ-CyD produced as the final product in eq 1 and this is given by eq 4.

$$[C_{60}^{\bullet-}/\gamma\text{-CyD}]_\infty = \frac{2k_{et}\tau_T[\text{NADH}]}{1 + k_{et}\tau_T[\text{NADH}]}\left(\frac{k_p}{k_p + k_b}\right)[^3C_{60}\text{*}/\gamma\text{-CyD}]_0 \quad (4)$$

According to eq 3, the pseudo-first-order decay rate constant of $^3C_{60}$*/γ-CyD (k_{obs}) increases linearly with an increase in the concentration of NADH with an intercept, which corresponds to τ_T^{-1}. This is confirmed as a linear plot of k_{obs} vs [NADH] in Figure 6. From the slope is obtained the k_{et} value as 1.0×10^8 M^{-1} s^{-1}. The τ_T value is obtained from the intercept as 33 μs which agrees with the literature value.[11,12]

By application of the steady-state approximation to the reactive species in Scheme 2, the dependence of the quantum yield (Φ) of formation of $C_{60}^{\bullet-}$/γ-CyD on [NADH] can be derived as given by eq 5 which predicts an increase in Φ with [NADH] to reach the limiting value Φ_∞ ($= 2k_p/(k_p + k_b)$).[39]

$$\Phi = \frac{2k_{et}\tau_T[\text{NADH}]}{1 + k_{et}\tau_T[\text{NADH}]}\left(\frac{k_p}{k_p + k_b}\right) \quad (5)$$

This relation is confirmed experimentally as shown in Figure 7a. The dependence of Φ on [NADH] is converted to a linear

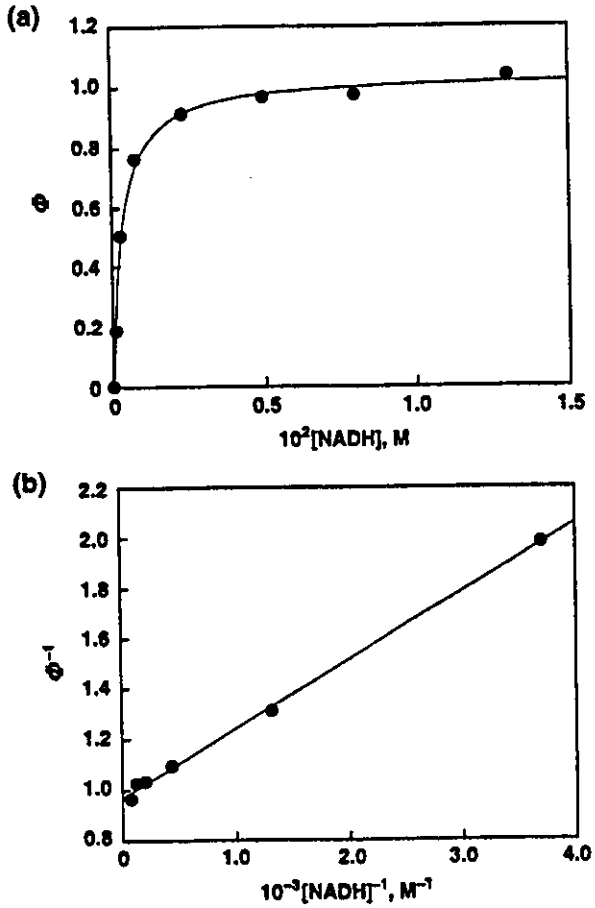

Figure 7. (a) Dependence of the quantum yield (Φ) on [NADH] for the photoreduction of C_{60}/γ-CyD (1.3×10^{-4} M) by NADH in deaerated phosphate buffer (50 mM, pH 7.4) at 298 K. (b) Plot of Φ^{-1} vs $[\text{NADH}]^{-1}$.

relation between Φ^{-1} and $[\text{NADH}]^{-1}$ (Figure 7b). From the slope and intercept are obtained the Φ_∞ and $k_{et}\tau_T$ values as 1.03 and 3.56×10^3 M^{-1}, respectively. The $k_p/(k_p + k_b)$ value is determined from the Φ_∞ value as 0.515. The k_{et} value is determined from the $k_{et}\tau_T$ value as 1.08×10^8 M^{-1} s^{-1} which agrees with the value (1.0×10^8 M^{-1} s^{-1}) determined directly from the appearance of $C_{60}^{\bullet-}$/γ-CyD in Figure 6. Such an agreement confirms the validity of Scheme 2.

Electron Transfer from $C_{60}^{\bullet-}$/γ-CyD to O_2. When O_2 is introduced to the aqueous solution containing $C_{60}^{\bullet-}$/γ-CyD formed in the photoreduction of C_{60}/γ-CyD by NADH, the absorption band at 1080 nm due to $C_{60}^{\bullet-}$/γ-CyD has disappeared immediately. Because the oxidation potential of $C_{60}^{\bullet-}$/γ-CyD (−0.56 V vs SCE)[34] is more negative than the reduction potential of O_2 (−0.40 V vs SCE),[35] electron transfer from $C_{60}^{\bullet-}$/γ-CyD to O_2 takes place to give C_{60}/γ-CyD and superoxide anion ($O_2^{\bullet-}$). In fact, $O_2^{\bullet-}$ was detected under visible-light irradiation of the aqueous C_{60}/γ-CyD-NADH-O_2 system by the ESR spin-trapping with use of DEPMPO as an $O_2^{\bullet-}$-trapping agent (vide supra). The long time scale observations of the time profiles of $C_{60}^{\bullet-}$/γ-CyD in the presence of different concentrations of molecular oxygen by the laser flash photolysis are shown in Figure 8 where the decay rate of the absorption due to $C_{60}^{\bullet-}$/γ-CyD at 1080 nm increases with increasing [O_2].

The mechanism for the C_{60}/γ-CyD-catalyzed generation of $O_2^{\bullet-}$ with NADH is shown in Scheme 3, where an energy transfer form $^3C_{60}$*/γ-CyD to O_2 (k_{EN}) and an electron transfer from $C_{60}^{\bullet-}$/γ-CyD to O_2 (k_{et}') are added to the mechanism for

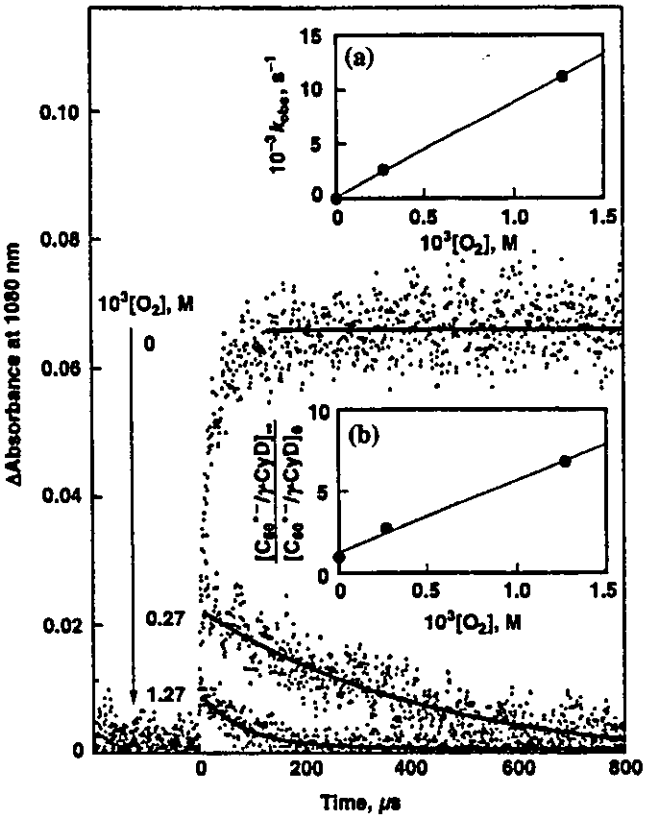

Figure 8. Time course changes of the absorbance at 1080 nm due to $C_{60}^{\bullet-}/\gamma$-CyD (5.5×10^{-5} M) in the presence of different concentration of O_2 in phosphate buffer (50 mM, pH 7.4) at 295 K. $[O_2] = 0$, 2.7×10^{-4}, 1.3×10^{-3} M. Insets: (a) plot of k_{obs} vs $[O_2]$; (b) plot of $[C_{60}^{\bullet-}/\gamma\text{-CyD}]_\infty/[C_{60}^{\bullet-}/\gamma\text{-CyD}]_0$ vs $[O_2]$.

SCHEME 3

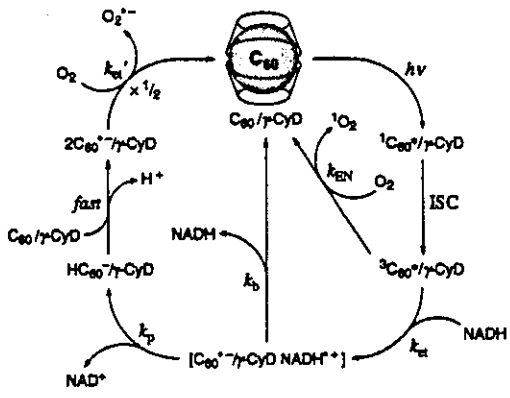

the photoreduction of C_{60} by NADH without O_2 (Scheme 2). According to Scheme 3, the decay of $C_{60}^{\bullet-}/\gamma$-CyD in the

$$[C_{60}^{\bullet-}/\gamma\text{-CyD}] = [C_{60}^{\bullet-}/\gamma\text{-CyD}]_0 \exp(-k_{et}'[O_2]t) \quad (6)$$

presence of O_2 is given by eq 6 where $[C_{60}^{\bullet-}/\gamma\text{-CyD}]_0$ is the initial concentration of $C_{60}^{\bullet-}/\gamma$-CyD in the presence of O_2 and is given by eq 7. In accordance with eq 6, the decay of $C_{60}^{\bullet-}/$

$$[C_{60}^{\bullet-}/\gamma\text{-CyD}]_0 = \frac{2k_{et}\tau_T[\text{NADH}][^3C_{60}^*/\gamma\text{-CyD}]_0}{1 + k_{et}\tau_T[\text{NADH}] + k_{EN}\tau_T[O_2]}\left(\frac{k_p}{k_p + k_b}\right) \quad (7)$$

γ-CyD obeys pseudo-first-order kinetics and the pseudo-first-order rate constant (k_{obs}) increases linearly with increasing $[O_2]$

TABLE 1: Observed Quantum Yields (Φ_{obs}) of Consumption of NADH in C_{60}/γ-CyD(1.3×10^{-4} M)-Photosensitized Reduction of O_2 by NADH in a Phosphate Buffer Solution (50 mM, pH 7.4) at 298 K and the Calculated Quantum Yields (Φ_{calc})

[NADH], M	$[O_2]$, M	Φ_{obs}	Φ_{calc}
7.5×10^{-4}	2.7×10^{-4}	0.22	0.16
9.8×10^{-4}	2.7×10^{-4}	0.24	0.19
1.2×10^{-3}	2.7×10^{-4}	0.25	0.22
5.5×10^{-4}	1.3×10^{-3}	0.12	0.10
8.3×10^{-4}	1.3×10^{-3}	0.16	0.13
1.1×10^{-3}	1.3×10^{-3}	0.18	0.17
1.4×10^{-3}	1.3×10^{-3}	0.20	0.20

as shown in the inset of Figure 8. From the slope of the linear plot of k_{obs} vs $[O_2]$ is obtained the k_{et}' value as 8.1×10^6 M^{-1} s^{-1}. The ratio of $[C_{60}^{\bullet-}/\gamma\text{-CyD}]_\infty$ in the absence of O_2 to $[C_{60}^{\bullet-}/\gamma\text{-CyD}]_0$ in the presence of O_2 is obtained from eqs 4 and 7 as given by eq 8. A linear correlation between $[C_{60}^{\bullet-}/\gamma\text{-CyD}]_\infty/[C_{60}^{\bullet-}/\gamma\text{-CyD}]_0$ and $[O_2]$ with the intercept of unity is confirmed as shown in Figure 8b. From the slope of the linear correlation in Figure 8b is obtained the k_{EN} value as 1.3×10^9 M^{-1} s^{-1}. This value agrees with the reported k_{EN} value (1.6×10^9 M^{-1} s^{-1}).[16]

$$[C_{60}^{\bullet-}/\gamma\text{-CyD}]_\infty/[C_{60}^{\bullet-}/\gamma\text{-CyD}]_0 = 1 + k_{EN}\tau_T[O_2]/(1 + k_{et}\tau_T[\text{NADH}]) \quad (8)$$

The reorganization energy for the self-exchange reaction of $O_2^{\bullet-}/O_2$ (λ_{11}) is derived from the Marcus equation,[40] as given by eq 9,[41] where $\Delta G^\ddagger$ is the activation free energy and λ_{22} is the reorganization energy for the self-exchange reaction of $C_{60}^{\bullet-}/C_{60}$. The λ_{22} value has previously been determined as 14.3 kcal mol^{-1}.[42]

$$\lambda_{11} = 2(2\Delta G^\ddagger - \Delta G^0_{et} + 2[\Delta G^\ddagger(\Delta G^\ddagger - \Delta G^0_{et})]^{1/2}) - \lambda_{22} \quad (9)$$

The $\Delta G^\ddagger$ value is obtained from the k_{et}' value using eq 10, where Z is the collision frequency taken as 1×10^{11} M^{-1} s^{-1} and the other notations are conventional. The λ_{11} value is determined as 43.4 kcal mol^{-1} from the $\Delta G^\ddagger$ and ΔG^0_{et} values using eq 9, This value agrees with the reported value of 45.5 kcal mol^{-1}

$$\Delta G^\ddagger = 2.3RT \log(Z/k_{et}') \quad (10)$$

which was directly determined utilizing ^{18}O as a probe for the self-exchange reaction between $^{36}O_2^{\bullet-}$ and $^{32}O_2$ in an aqueous solution.[43] Such an agreement indicates that an electron transfer from $C_{60}^{\bullet-}/\gamma$-CyD to O_2 undergoes via an outer-sphere pathway.

$O_2^{\bullet-}$ Formation via $^1O_2$. Singlet oxygen ($^1O_2$: $^1\Delta_g$) produced in an energy transfer from $^3C_{60}^*$ to O_2 in Scheme 3 may also be reduced by NADH to $O_2^{\bullet-}$.[44] Thus, the oxidation of NADH by $^1O_2$ as well as $^3C_{60}^*/\gamma$-CyD is examined by determining the quantum yield (Φ) of the C_{60}/γ-CyD-photosensitized oxidation of NADH by O_2. The observed Φ values (Φ_{obs}) were determined from the disappearance of the absorption due to NADH at 380 nm at different concentrations of NADH and O_2 (see Experimental Section) and the results are listed in Table 1.

In general, $^1O_2$ is quenched by physical and chemical processes in which only the latter gives the actual products.[45,46] A laser flash photolysis study by Peters et al.[44] has revealed that $^1O_2$ is quenched by both the physical and electron-transfer processes in competition with the decay of $^1O_2$ to the ground state (the lifetime τ in H_2O is 4.2 μs)[46] as shown in Scheme 4. The physical quenching process gives the ground-state reactant

SCHEME 4

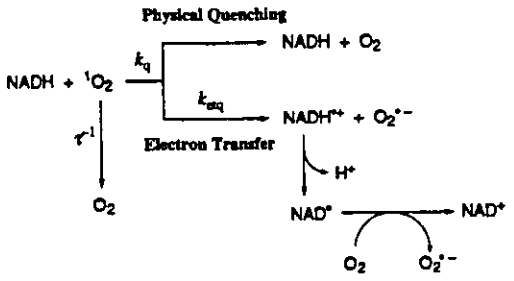

pair, NADH and O_2, whereas the electron transfer produces $NADH^{\bullet+}$ and $O_2^{\bullet-}$. The deprotonation of NADH is followed by the second electron transfer to O_2 to produce NAD^+ and $O_2^{\bullet-}$ with a rate constant of 1.9×10^9 M^{-1} s^{-1}.[47] The total quenching constant (k_q) and the electron-transfer quenching rate constant (k_{etq}) have been determined as 7.9×10^7 M^{-1} s^{-1} and 4.3×10^7 M^{-1} s^{-1}, respectively.[44]

By combining Scheme 3 and Scheme 4, the quantum yield (Φ) of the C_{60}/γ-CyD-photosensitized oxidation of NADH by O_2 is derived as given by eq 11 (see Supporting Information for the derivation). The first term corresponds to a direct photoinduced electron-transfer pathway to $^3C_{60}$*/γ-CyD and the second term corresponds to a $^1O_2$ pathway. Because all the rate

$$\Phi = \frac{k_{et}\tau_T[\mathrm{NADH}]}{1 + k_{et}\tau_T[\mathrm{NADH}] + k_{EN}\tau_T[O_2]}\left(\frac{k_p}{k_p + k_b}\right) + \frac{k_{etq}\tau[\mathrm{NADH}]}{1 + k_q\tau[\mathrm{NADH}]}\frac{k_{EN}\tau_T[O_2]}{1 + k_{et}\tau_T[\mathrm{NADH}] + k_{EN}\tau_T[O_2]} \quad (11)$$

constants in eq 11 are known or determined in this study, the Φ value can be calculated using eq 11. The calculated Φ values (Φ_{calc}) are listed in Table 1, where they agree well with the experimental values (Φ_{obs}). Such an agreement confirms the validity of Schemes 3 and 4. The Φ_{calc} values in Table 1 are those corresponding to a direct photoinduced electron-transfer pathway. As expected from Schemes 3 and 4, the photoinduced electron-transfer pathway becomes important with increasing the NADH concentration but the $^1O_2$ pathway (Scheme 4) dominates with increasing the O_2 concentration.

Actual Reactive Species for DNA Cleavage. As described above, the C_{60}/γ-CyD-photosensitized reduction of O_2 by NADH gives $O_2^{\bullet-}$ via both a direct photoinduced electron transfer from NADH to $^3C_{60}$*/γ-CyD (Scheme 3) and an electron transfer from NADH to $^1O_2$ produced in an energy transfer from $^3C_{60}$* to O_2 (Scheme 4). Formation of $O_2^{\bullet-}$ may be inhibited by addition of NaN_3 which can quench $^3C_{60}$*/γ-CyD in competition with an electron transfer from NADH and an energy transfer to O_2. In fact, $^3C_{60}$*/γ-CyD is significantly quenched by NaN_3 as shown in Figure 9. The decay rate obeys pseudo-first-order kinetics and the pseudo-first-order decay rate constant of $^3C_{60}$*/γ-CyD (k_{obs}) increases linearly with an increase in the concentration of NaN_3 (inset of Figure 9). From the slope of the linear plot is determined the quenching rate constant by NaN_3 as 1.7×10^8 M^{-1} s^{-1}.

This value is larger than the k_{et} value of an electron transfer from NADH to $^3C_{60}$*/γ-CyD (1.0×10^8 M^{-1} s^{-1}), indicating that NaN_3, which is known as an efficient $^1O_2$ scavenger, can also act as a quencher of the triplet excited state $^3C_{60}$*/γ-CyD itself. In such a case, photocleavage of DNA is also inhibited by adding sodium azide (NaN_3) as shown Figure 10 (lane 2 in reference to lane 1).

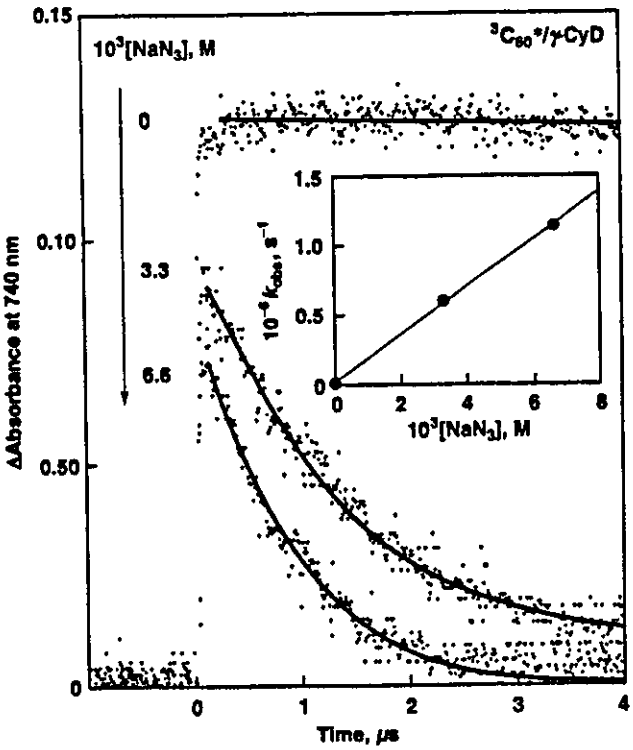

Figure 9. Time course changes of the absorbance at 740 nm due to $^3C_{60}$*/γ-CyD (5.5×10^{-5} M) in the presence of different concentration of NaN_3 in phosphate buffer (50 mM, pH 7.4) at 295 K. [NaN_3] = 0, $0.3.3 \times 10^{-3}$, 6.6×10^{-3} M. Insets: plot of k_{obs} vs [NaN_3].

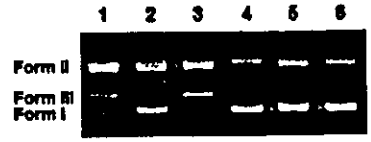

Figure 10. The effect of various additives on the DNA-cleaving activities of C_{60}/γ-CyD-NADH-O_2 system in phosphate buffer (50 mM, pH 7.4) after 1 h visible-light irradiation with 300-W reflector lamp at 273 K. Lane 1: C_{60}/γ-CyD (4.6×10^{-5} M) + NADH (1.0×10^{-2} M) (standard cleavage reaction). Lanes 2–6, standard reaction with additives: lane 2, with NaN_3 (1.0×10^{-2} M); lane 3, with SOD (100 μg mL^{-1}); lane 4, with catalase (100 μg mL^{-1}); lane 5, with methanol (1 M); lane 6, with ethanol (1 M).

SCHEME 5

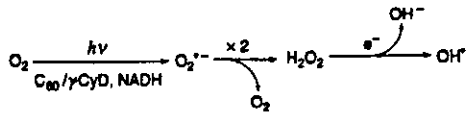

Thus, formation of $O_2^{\bullet-}$ via $^3C_{60}$*/γ-CyD may play an essential role in the DNA cleavage. However, this does not necessarily mean that $O_2^{\bullet-}$ is an actual reactive species for the DNA cleavage because $O_2^{\bullet-}$ is generally regarded as a rather unreactive radical species.[36] To examine the actual role of $O_2^{\bullet-}$ in the DNA cleavage, the DNA cleavage activity of the C_{60}/γ-CyD-NADH-O_2 system was determined in the presence of the enzyme superoxide dismutase (SOD). Addition of SOD shows no inhibitory effect on DNA cleavage as shown in Figure 10 (lane 3 in reference to lane 1). This indicates that H_2O_2 produced via disproportionation of $O_2^{\bullet-}$ is responsible for the DNA cleavage (Scheme 5). Such an SOD-dependent increase in DNA cleavage has been observed in other systems where $O_2^{\bullet-}$ is formed in the presence of electron donors.[48] Addition of the H_2O_2-destroying enzyme catalase significantly inhibits DNA cleavage (lane 4 in Figure 10). Addition of hydroxyl

radical (•OH) scavengers such as methanol (lane 5) and ethanol (lane 6) also inhibits DNA cleavage. The •OH is known as one of the most noxious reactive oxygen species, which induces the DNA cleavage.[49] The •OH can be produced in a trace-metal-dependent Fenton reaction of H_2O_2 (Scheme 5) as reported for the DNA cleavage by the antitumor antibiotic leinamycin.[50] Thus, any reagent that is capable of reducing oxygen to superoxide anion can produce hydroxyl radical.[49d] Thus, the actual reactive species for the photoinduced DNA cleavage in the aqueous C_{60}/γ-CyD-NADH-O_2 system may be hydroxyl radical as shown in Scheme 5.

In conclusion, the C_{60}/γ-CyD-photosensitized reduction of O_2 by NADH produces $O_2^{\bullet-}$ efficiently via a direct photoinduced electron transfer from NADH to $^3C_{60}^*/\gamma$-CyD (Scheme 3) and via an electron transfer from NADH to $^1O_2$ produced by an energy transfer from $^3C_{60}^*/\gamma$-CyD to O_2 (Scheme 4). The contribution of the former process increases with increasing the NADH concentration and the latter dominates with increasing the O_2 concentration. The $O_2^{\bullet-}$ thus produced gives H_2O_2, ultimately yielding hydroxyl radical (Scheme 5) which is an actual DNA-cleaving reagent.

Acknowledgment. This work was partially supported by a Grant-in-Aid for Scientific Research Priority Area (No. 11228205) from the Ministry of Education, Culture, Sports, Science and Technology, Japan.

Supporting Information Available: Dose-dependences of C_{60}/γ-CyD and NADH on DNA cleavage (Figure S1) and derivation of eq 11 (2 pages). This material is available free of charge via the Internet at http://pubs.acs.org.

References and Notes

(1) (a) Arbogast, J. W.; Darmanyan, A. P.; Foote, C. S.; Rubin, Y.; Diedrich, F. N.; Alverez, M. M.; Anz, S. J.; Whetten, R. L. *J. Phys. Chem.* **1991**, *95*, 11. (b) Arbogast, J. W.; Foote, C. S. *J. Am. Chem. Soc.* **1991**, *113*, 8886.

(2) Nagano, T.; Arakane, K.; Ryu, A.; Masunaga, T.; Shinmoto, K.; Mashiko, S.; Hirobe, M. *Chem. Pharm. Bull.* **1994**, *42*, 2291.

(3) Wilson, S. R. In *Fullerenes: Chenistry, Physics, and Technology*; Kadish, K. M., Ruoff, R. S., Eds.; Wiley: New York, 2000; pp 437−465.

(4) (a) Jensen, A. W.; Wilson, S. R.; Schuster, D. I. *Bioorganic Med. Chem.* **1996**, *4*, 767. (b) Da Ros, T.; Prato, M. *Chem. Commun.* **1999**, 663. (c) Xu, Z.; Suo, Z. Y.; Wei, X. W.; Zhu, D. X. *Prog. Biochim. Biophys.* **1998**, *25*, 130.

(5) Wan, S.; Parrish, J. A.; Anderson, R. R.; Madden, M. *Photochem. Photobiol.* **1981**, *34*, 679.

(6) (a) Tsuchiya, T.; Yamakoshi, Y. N.; Miyata, N. *Biochem. Biophys. Res. Commun.* **1995**, *206*, 885. (b) Tsuchiya, T.; Oguri, I.; Yamakoshi, Y. N.; Miyata, N. *Fullerene Sci. Technol.* **1996**, *4*, 989.

(7) HIV-1 protease inhibition: (a) Friedman, S. H.; DeCamp, D. L.; Sijbesma, R. P.; Srdanov, G.; Wudl, F.; Kenyon, G. L. *J. Am. Chem. Soc.* **1993**, *115*, 6505. (b) Toniolo, C.; Bianco, A.; Maggini, M.; Scorrano, G.; Prato, M.; Marastoni, M.; Tomatis, R.; Spisani, S.; Palú, R.; Blair, E. D. *J. Med. Chem.* **1994**, *37*, 4558. Glutathione *S*-transferase inhibition: (c) Iwata, N.; Mukai, T.; Yamakoshi, Y.; Hara, S.; Yanase, T.; Shoji, M.; Endo, T.; Miyata, N. *Fullerene Sci. Technol.* **1998**, *6*, 213.

(8) (a) Chiang, L. Y.; Lu, F.-J.; Lin, J.-T. *J. Chem. Soc., Chem. Commun.* **1995**, 1283. (b) Lai, Y.-L.; Chiou, W.-Y.; Chiang, L. Y. *Fullerene Sci. Technol.* **1997**, *5*, 1057.

(9) (a) Tokuyama, H.; Yamago, S.; Nakamura, E.; Shiraki, T.; Sugiura, Y. *J. Am. Chem. Soc.* **1993**, *115*, 7918. (b) Boutorine, A. S.; Tokuyama, H.; Takasugi, M.; Isobe, H.; Nakamura, E.; Hélène, C. *Angew. Chem., Int. Ed. Engl.* **1994**, *33*, 2462. (c) Irie, K.; Nakamura, Y.; Ohigashi, H.; Tokuyama, H.; Yamago, S.; Nakamura, E. *Biosci. Biotechnol, Biochem.* **1996**, *60*, 1359. (d) Nakamura, E.; Tokuyama, H.; Yamago, S.; Shiraki, T.; Sugiura, Y. *Bull. Chem. Soc. Jpn.* **1996**, *69*, 2143.

(10) An, Y.-Z.; Chen, C.-H. B.; Anderson, J. L.; Sigman, D. S.; Foote C. S.; Rubin, T. *Tetrahedron* **1996**, *52*, 5179.

(11) (a) Yamakoshi, Y.; Sueyoshi, S.; Fukuhara, K.; Miyata, N.; Masumizu, T.; Kohno, M. *J. Am. Chem. Soc.* **1998**, *120*, 12363. (b) Yamakoshi, Y.; Yagami, T.; Sueyoshi, S.; Miyata, N. *J. Org. Chem.* **1996**, *61*, 7236. (c) Sera, N.; Tokiwa, H.; Miyata, N. *Carcinogenesis* **1996**, *17*, 2163.

(12) Foote, C. S. *Top. Curr. Chem.* **1994**, *169*, 347.

(13) Arbogast, J. W.; Foote, C. S.; Kao, M. *J. Am. Chem. Soc.* **1992**, *114*, 2277.

(14) Fukuzumi, S.; Guldi, D. M. In *Electron Transfer in Chemistry*; Balzani, V., Ed.; Wiley-VCH: Weinheim, 2001; Vol. 2, pp 270−337.

(15) (a) Fujitsuka, M.; Luo, C.; Ito, O. *J. Phys. Chem. B* **1999**, *103*, 445. (b) Luo, C.; Fujitsuka, M.; Huang, C.-H.; Ito, O. *J. Phys. Chem. A* **1998**, *102*, 8716. (c) Luo, C.; Fujitsuka, M.; Huang, C.-H.; Ito, O. *Phys. Chem. Chem. Phys.* **1999**, *1*, 2923. (d) Rath, M. C.; Pal, H.; Mukherjee, T. *J. Phys. Chem. A* **1999**, *103*, 4993.

(16) Guldi, D. M.; Kamat, P. V. In *Fullerenes: Chemistry, Physics, and Technology*; Kadish, K. M., Ruoff, R. S., Eds.; Wiley: New York; 2000, pp 225−281.

(17) (a) Ghosh, H. N.; Pal, H.; Sapre, A. V.; Mittal, J. P. *J. Am. Chem. Soc.* **1993**, *115*, 11 722. (b) Fukuzumi, S.; Suenobu, T.; Patz, M.; Hirasaka, T.; Itoh, S.; Fujitsuka, M.; Ito, O. *J. Am. Chem. Soc.* **1998**, *120*, 8060. (c) Fukuzumi, S.; Suenobu, T.; Fujitsuka, M.; Ito, O.; Tonoi, T.; Matsumto, S.; Mikami, K. *J. Organomet. Chem.* **1999**, *574*, 32. (d) Mikami, K.; Matsumoto, S.; Okubo, Y.; Fujitsuka, M.; Ito, O.; Suenobu, T.; Fukuzumi, S. *J. Am. Chem. Soc.* **2000**, *122*, 2236.

(18) Reed, C. A.; Bolskar, R. D. *Chem. Rev.* **2000**, *100*, 1075.

(19) Fukuzumi, S.; Mori, H.; Suenobu, T.; Imahori, H.; Gao, X.; Kadish, K. M. *J. Phys. Chem. A* **2000**, *104*, 10 688.

(20) Bernstein, R.; Prat, F.; Foote, C. S. *J. Am. Chem. Soc.* **1999**, *121*, 464.

(21) Sheu, C.; Foote, C. S. *J. Am. Chem. Soc.* **1995**, *117*, 6439.

(22) (a) Fujitsuka, M.; Ito, O.: Yamashiro, T.; Aso, Y.; Otsubo, T. *J. Phys. Chem. A* **2000**, *104*, 4876. (b) Ito, O.; Yamazaki, M.; Fujitsuka, M. In *Fullerenes 2000 Volume 8: Electrochemistry and Photochemistry*; Fukuzumi, S., D'Souza, F., Guldi, D. M., Eds.; The Electrochemical Soceity: Pennington, 2000; pp 306−318.

(23) (a) Andersson, T.; Nilsson, K.; Sundahl, M.; Westman, G.; Wennerström, O. *J. Chem. Soc., Chem. Commun.* **1992**, 604. (b) Kutner, W.; Boulas, P.; Kadish, K. M. *J. Electrochem. Soc.* **1992**, *139*, 243C. (c) Sundahl, M.; Andersson, T.; Nilsson, K.; Wennerström, O.; Westman, G. *Synth. Met.* **1993**, *55−57*, 3252. (d) Andersson, T.; Westman, G.; Wennerström, O.; Sundahl, M. *J. Chem. Soc., Perkin Trans. 2* **1994**, 1097. (e) Boulas, P.; Kutner, W.; Jones, M. T.; Kadish, K. M. *J. Phys. Chem.* **1994**, *98*, 1282. (f) Priyadarsini, K. I.; Mohan, H.; Mittal, J. P. *Fullerene Sci. Technol.* **1995**, *3*, 479. (g) Yoshida, Z.; Takekuma, H.; Takekuma, S.; Matsubara, Y. *Angew. Chem., Int. Ed. Engl.* **1994**, *33*, 1597. (h) Buvari-Barcza, A.; Barcza, L.; Braun, T.; *Supramol. Chem.* **1994**, *4*, 131. (i) Buvari-Barcza, A.; Barcza, L.; Braun, T.; Konkoly-Thege, I.; Ludanyi, K.; Vekey, K. *Fullerene Sci. Technol.* **1997**, *5*, 331. (j) Braun, T. *Fullerene Sci. Technol.* **1997**, *74*, 47.

(24) Ohlendorf, V.; Willnow, A.; Hungerbühler, H.; Guldi, D. M.; Asmus, K.-D. *J. Chem. Soc., Chem. Commun.* **1995**, 759.

(25) (a) Priyadarsini, K. I.; Mohan, H.; Mittal, J. P.; Guldi, D. M.; Hungerbühler, H.; Asmus, K.-D. *J. Phys. Chem.* **1994**, *98*, 9565. (b) Priyadarsini, K. I.; Mohan, H.; Tyagi, A. K.; Mittal, J. P. *J. Phys. Chem.* **1994**, *98*, 4756.

(26) Yamakoshi, Y. N.; Yagami, T.; Fukuhara, K.; Sueyoshi, S.; Miyata, N. *J. Chem. Soc., Chem. Commun.* **1994**, 517.

(27) (a) Frejaville, C.; Karoui, H.; Tuccio, B.; Lemoigne, F.; Culcasi, M.; Pietri, S.; Lauricella, R.; Tordo, P. *J. Med. Chem.* **1995**, *38*, 258. (b) Karoui, H.; Hogg, N.; Fréjaville, C.; Tordo, P.; Kalyanaraman, B. *J. Biol. Chem.* **1996**, *271*, 6000. (c) Vásquez-Vivar, J.; Hogg, N.; Pritchard, Jr., K. A.; Martasek, P.; Kalyanaraman, B. *FEBS Lett.* **1997**, *404*, 127.

(28) (a) Komatsu, K.; Fujiwara, K.; Murata, Y.; Braun, T. *J. Chem. Soc., Perkin Trans. 1* **1999**, 2963. (b) Braun, T.; Buvari-Barcza, A.; Barcza, L.; Konkoly-Thege, I.; Fodor, M.; Migali, B. *Solid State Ionics* **1994**, *74*, 47.

(29) Masuhara, A.; Fujitsuka, M.; Ito, O. *Bull. Chem. Soc. Jpn.* **2000**, *73*, 2199.

(30) Watanabe, A.; Ito, O *J. Phys. Chem.* **1994**, *98*, 7736.

(31) Konishi, T.; Sasaki, Y.; Fujitsuka, M.; Toba, Y.; Moriyama, H.; Ito, O. *J. Chem. Soc., Perkin Trans. 2* **1999**, 551.

(32) (a) Hatchard, C. G.; Parker, C. A. *Proc. R. Soc. London, Ser. A* **1956**, *235*, 518. (b) Calvert, J. G.; Pitts, J. N. In *Photochemistry*; Wiley: New Tork, 1966; p 783.

(33) Lawson, D. R.; Feldheim, D. L.; Foss, C. A.; Dorhout, P. K.; Elliot, C. M.; Martin, C. R.; Parkinson, B. *J. Electrochem. Soc.* **1992**, *139*, L68.

(34) Lion, Y.; Delmelle, M.; Van De Vorst, A. *Nature* **1976**, *263*, 442.

(35) Ohlendorf, V.; Willnow, A.; Hungerbühler, H.; Guldi, D. M.; Asmus, K.-D. *J. Chem. Soc., Chem. Commun.* **1995**, 759.

(36) Sawyer, D. T.; Roberts, J. L., Jr. *Acc. Chem. Res.* **1988**, *21*, 469.

(37) The same stoichiometry of the photoreduction of C_{60} by an NADH model compound has been established previously, see: ref 17b.

(38) Fukuzumi, S.; Suenobu, T.; Hirasaka, T.; Sakurada, N.; Arakawa, R.; Fujitsuka, M.; Ito, O. *J. Phys. Chem. A* **1999**, *103*, 5935.

(39) For the derivation, see the Supporting Information.

(40) (a) Marcus, R. A. *Annu. Rev. Phys. Chem.* **1964**, *15*, 155. (b) Marcus, R. A. *Angew. Chem., Int. Ed. Engl.* **1993**, *32*, 1111.

(41) Fukuzumi, S.; Nakanishi, I.; Tanaka, K.; Suenobu, T.; Tabard, A.; Guilard, R.; Van Caemelbecke, E.; Kadish, K. M. *J. Am. Chem. Soc.* **1999**, *121*, 785.

(42) Fukuzumi, S.; Nakanishi, I.; Suenobu, T.; Kadish, K. M. *J. Am. Chem. Soc.* **1999**, *121*, 3468.

(43) Lind, J.; Shen, X.; Merényi, G.; Jonsson, B. Ö. *J. Am. Chem. Soc.* **1989**, *111*, 7654.

(44) Peters, G.; Rodgers, M. A. J. *Biochim. Biophys. Acta* **1981**, *637*, 43.

(45) (a) Foote, C. S. *Acc. Chem. Res.* **1968**, *1*, 104. (b) Kearns, D. R. *Chem. Rev.* **1971**, *71*, 395. (d) Stephenson, L. M.; Grdina, M. J.; Orfanopoulos, M. *Acc. Chem. Res.* **1980**, *13*, 419. (e) Foote, C. S.; Clennan, E. L. *Properties and Reactions of Singlet Oxygen. In Active Oxygen in Chemistry*; Foote, C. S., Valentine, J. S., Greenberg, A., Liebman, J. F., Eds.; Chapman and Hall: London, 1995; pp 105−140.

(46) Wilkinson, F.; Helman, W. P.; Ross, A. B. *J. Phys. Chem. Ref. Data* **1995**, *24*, 663.

(47) Willson, R. L. *Chem. Commun.* **1970**, 1005.

(48) (a) Eliot, H.; Gianni, L.; Myers, C. *Biochemistry* **1984**, *23*, 928. (b) Nagai, K.; Hecht, S. M. *J. Biol. Chem.* **1991**, *266*, 23 994. (c) Parraga, A.; Orozco, M.; Portugal, J. *Eur. J. Biochem.* **1992**, *208*, 227.

(49) (a) von Sonntag, C. *The Chemical Basis of Radiation Biology*; Talor & Francis: London, 1987. (b) Pogozelski, W. K.; Tullius, T. D. *Chem. Rev.* **1998**, *98*, 1089. (c) Burrows, C. J.; Muller, J. G. *Chem. Rev.* **1998**, *98*, 1109. (d) Armitage, B. *Chem. Rev.* **1998**, *98*, 1171.

(50) (a) Mitra, K.; Kim, W.; Daniels, J. S.; Gates, K. S. *J. Am. Chem. Soc.* **1997**, *119*, 11 691. (b) Behroozi, S. J.; Kim, W.; Dannaldson, J.; Gates, K. S. *Biochemistry* **1996**, *35*, 1768.

J|A|C|S
COMMUNICATIONS

Published on Web 05/07/2002

Enhanced Radical-Scavenging Activity of a Planar Catechin Analogue

Kiyoshi Fukuhara,*,† Ikuo Nakanishi,†,‡ Hisao Kansui,† Etsuko Sugiyama,§ Mitsuhiro Kimura,∥ Tomokazu Shimada,∥ Shiro Urano,∥ Kentaro Yamaguchi,⊥ and Naoki Miyata#

Division of Organic Chemistry, National Institute of Health Sciences, Setagaya-ku, Tokyo 158-8501, Redox Regulation Research Group, National Institute of Radiological Sciences, Japan Science and Technology Corporation (JST), Inage-ku, Chiba 263-8555, Showa Wemen's University, Setagaya-ku, Tokyo 154-8533, Department of Applied Chemistry, Shibaura Institute of Technology, Minato-ku, Tokyo 108-8548, Chemical Analysis Canter, Chiba University, JST, Inage-ku, Chiba 263-8522, and Graduate School of Pharmaceutical Sciences, Nagoya City University, Mizuho-ku, Nagoya 467-8603, Japan

Received December 20, 2001

Oxidative stress is important in the pathogenesis of neuronal cell death in Alzheimer's[1] and Parkinson's[2] disease. The protective role of antioxidants against such pathogens has been widely studied, and this has promoted the development of antioxidants for the treatment of diseases associated with oxidative stress.[3-5] Vitamin E, which is an essential nutrient in humans, may be a clinically useful antioxidant. In fact, α-tocopherol reduces amyloid-induced cell death and suppresses the progression of Alzheimer's disease.[3] Flavonoids such as catechin (**1**) and quercetin (**2**) are plant phenolic pigment products that act as natural antioxidants. Quercetin, on one hand, has been shown to protect against oxidant injury and cell death[6] by scavenging free radicals,[7] protecting against lipid peroxidation,[8] and thereby terminating the chain-radical reaction.[9] On the other hand, there have been only a few reports on the use of catechin for the treatment of free radical-associated disease, whereas the mechanism to scavenge oxygen radical has been well-studied.[10] However, its ability to scavenge free radicals must be improved, and adequate lipophilicity is needed to penetrate the cell membrane before it is suitable for clinical use. The superior antioxidant ability of **2** results from the formation of a stable radical, due to the C2−C3 double bond and the resulting planar geometry which delocalizes the radical throughout the entire molecule.[11] Since the B ring in **1** is known to be perpendicular to the A ring,[12] the radical-scavenging ability of **1** might be improved by constraining the geometry of **1** to be planar. In this communication, we describe the first synthesis and characterization of the antioxidant properties of a planar catechin analogue (**3**) with respect to the chroman and catechol moieties of **1**, by taking advantage of the formation of a bridge between the 3-OH group on ring C and C6′ on ring B.

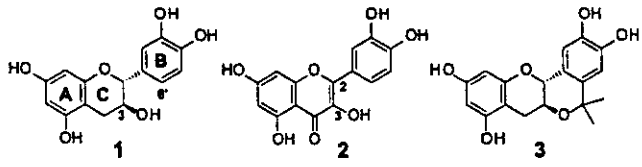

The planar catechin (**3**) was synthesized via an oxa-Pictet−Spengler reaction[13] using catechin and acetone with $BF_3 \cdot Et_2O$ as the acid. The structure was characterized by ^1H and ^{13}C NMR and

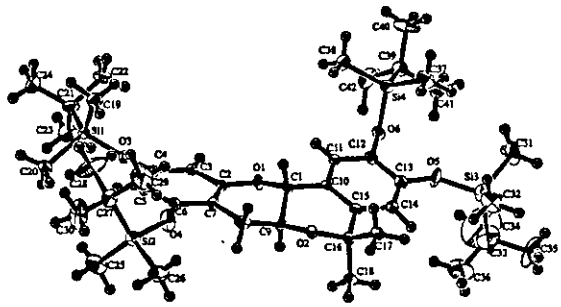

Figure 1. X-ray structure of tetra-*O*-silylated analogue (**4**) of **3**, showing ellipsoids at 50% probability.

UV−visible spectroscopy. The ^1H signals of the four protons of the phenolic OH groups showed that the catechol moiety on ring B did not react with acetone. As shown in Figure 1, the planar geometry of **3** was substantiated by single-crystal X-ray crystallography of a tetra-*O*-silylated analogue (**4**), in which the four OH groups on the A and B rings are substituted by *t*-Bu(Me)$_2$SiO groups. X-ray analysis also confirmed that the stereochemistry of 3-H on ring C was maintained throughout the reaction without any acid-catalyzed racemization.

The radical-scavenging activities of **1** and **3** as well as that of **2** were compared using galvinoxyl radical (G•) as an oxyl radical species.[14] Upon addition of **1** to a deaerated MeCN solution of G•, the absorption band at 428 nm due to G• disappeared immediately as shown in Figure 2. This indicates that hydrogen abstraction from one of the OH groups on the B ring of **1** by G• takes place to give catechin radical and hydrogenated G• (GH). The decay of the absorbance at 428 nm due to G• obeyed pseudo-first-order kinetics when the concentration of **1** was maintained at more than 10-fold excess of the G• concentration (inset of Figure 2). The dependence of the observed pseudo-first-order rate constant (k_{obs}) on the concentration of **1** is shown in Figure 3, which demonstrates a linear correlation between k_{obs} and the concentration of **1**. From the linear plot of k_{obs} vs the catechin concentration in Figure 3, we determined that the second-order rate constant (k) for hydrogen abstraction of **1** by G• was 2.34×10^2 M^{-1} s^{-1}. The k values for **2** and **3** were determined in the same manner to be 1.08×10^3 and 1.12×10^3 M^{-1} s^{-1}, respectively. Thus, the k value for planar catechin (**3**) is about 5-fold larger than that for catechin (**1**), approximately the same as that for quercetine (**2**).

Hydroxyl radical is the most reactive among oxygen-derived free radicals responsible for aging and free radical-mediated injury. Therefore, the effects of **1**, **2**, and **3** on hydroxyl radical-mediated

* To whom correspondence should be addressed. E-mail: fukuhara@nihs.go.jp.
† National Institute of Health Sciences.
‡ National Institute of Radiological Sciences, Japan Science and Technology Corporation.
§ Showa Wemen's University.
∥ Shibaura Institute of Technology.
⊥ Chiba University, Japan Science and Technology Corporation.
Nagoya City University.

10.1021/ja0178259 CCC: $22.00

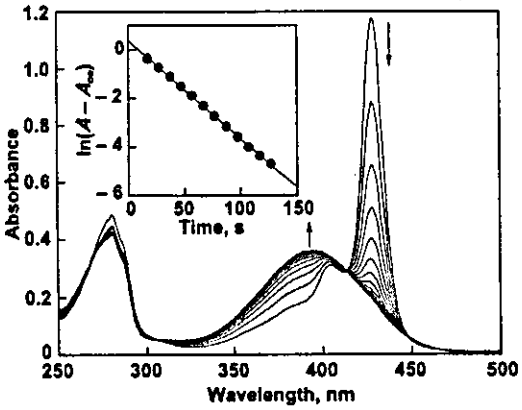

Figure 2. Spectral change in the reaction of **1** (1.5×10^{-4} M) with G• (2.4×10^{-6} M) in deaerated MeCN at 298 K (Interval: 10 s). (Inset) First-order plot based on the change in absorption at 428 nm.

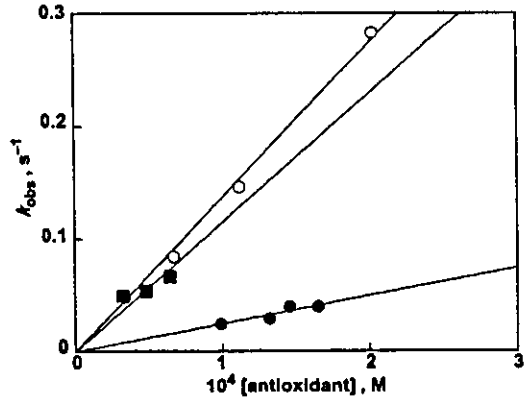

Figure 3. Plot of the pseudo-first-order rate constant (k_{obs}) vs the concentrations of **1** (●), **2** (■), and **3** (○) for hydrogen atom transfer from antioxidants to G• (2.4×10^{-6} M) in deaerated MeCN at 298 K.

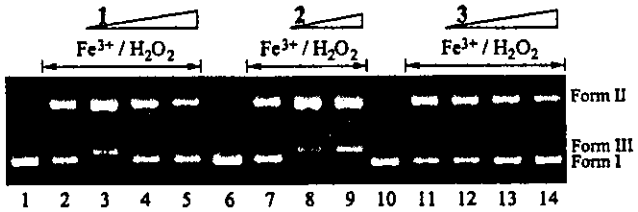

Figure 4. Effects of **1**, **2**, and **3** on DNA breakage induced by Fe^{3+}/H_2O_2. Assays were performed in 50 mM sodium cacodylate buffer, pH 7.2, containing 45 μM bp of pBR322DNA, for 1 h at 37 °C. Lanes 1, 6, and 10; DNA alone, lanes 2, 7, and 11; 10 mM H_2O_2 and 10 μM $FeCl_3$, lanes 3−5, 8, and 9, and 12−14; 10 mM H_2O_2 and 10 μM $FeCl_3$ in the presence of 0.25, 1.25, and 2.5 mM **1** (lanes 3−5), 0.25 and 1.25 mM **2**, and 0.25, 1.25 and 2.5 mM **3**.

DNA breakage were investigated. DNA-strand scission in supercoiled pBR322DNA was induced by a hydroxyl radical-generating system using hydrogen peroxide in the presence of Fe^{3+} (Fenton reaction). As shown in Figure 4, **1** at a high concentration (1.25 and 2.5 mM) suppressed DNA strand breakage, while at a low concentration (0.25 mM) it exhibited pro-oxidant properties, consistent with the enhanced DNA cleavage in comparison with cleavage without antioxidant. Quercetin (**2**) only showed pro-oxidant effects at 0.25 and 1.25 mM. In agreement with previously published results,[15] the measured pro-oxidant effects of **1** and **2** may be attributed to autoxidation of the antioxidant in the presence of transition metal, leading to the generation of primary radicals such as hydroxyl radical. In contrast to the pro-oxidant effects of **1** and **2**, the addition of **3** protected DNA from Fenton reaction-mediated damage at all of the concentrations tested, and **3** exhibited marked hydroxyl radical-scavenging ability, which exceeded that of catechin. Since **3** is very lipophilic compared to **1** (data not shown), the high radical-scavenging ability of **3** might be very useful for suppressing free-radical associated events, especially in the cell membrane.

In conclusion, we have described the first synthesis of planar catechin **3**, which was constrained by the formation of a bridge between the 3-OH group on ring C and C6′ on ring B. Preliminary experiments indicated that, despite the absence of a C2−C3 double bond, **3** showed enhanced radical-scavenging ability comparable to that of **2**. Efficient protection against DNA strand breakage induced by the Fenton reaction and the greater lipophilicity of **3** suggested that the construction of a planar catechin might be a new approach for the development of clinically useful antioxidants. The inducing planarity of **3** may pose the preferential stabilization of radicals through hyperconjugation between the π electrons on ring B and the σ electrons on C2 on ring C. In fact, a large amount of the spin density in the radical species generated via the antioxidative reaction of **3** is accumulated at the C2 position (data not shown). However, the effect of substitution to the para position from an OH ring on the B ring also should be considered as the essential factor for its enhanced reactivity. The detailed mechanism as well as the energetics of hydrogen abstraction from catechin analogues depending on the molecular structure is now under investigation.

Supporting Information Available: Experimental procedure for the preparation of **3**, kinetic measurements, the DNA-cleaving experiment, and crystallographic data for **4** (PDF). This material is available free of charge via the Internet at http://pubs.acs.org.

References

(1) (a) Katzman, R.; Kawas, C. In *Alzheimer Disease*; Terry, R. D, Katzman, R., Bick, K. L., Eds.; Raven Press: New York, 1994; pp103−119. (b) Behl, C.; Davis, J. B.; Lesley, R.; Schubert, D. *Cell* **1994**, *77*, 817. (c) Butterfield, D. A. *Chem. Res. Toxicol.* **1997**, *10*, 495. (d) Huang, X.; Atwood, C. S.; Hartshorn, M. A.; Multhaup, G.; Goldstein, L. E.; Scarpa, R. C.; Cuajungco, M. P.; Gray, D. N.; Lim, J.; Moir, R. D.; Tanzi, R. E.; Bush, A. I. *Biochemistry* **1999**, *38*, 7609.

(2) (a) Olanow, C. W. *Neurology* **1990**, *40*, 37. (b) Zang, L.-Y.; Misra, H. P. *J. Biol. Chem.* **1992**, *267*, 23601. (c) Pennathur, S.; Jackson-Lewis, V.; Przedborski, S.; Heinecke, J. W. *J. Biol. Chem.* **1999**, *274*, 34621.

(3) (a) Mayeux, R.; Sano, M. J. *N. Engl. J. Med.* **1999**, *341*, 1670. (b) Grundman, M. *Am. J. Clin. Nutr.* **2000**, *71*, 630S.

(4) (a) Skaper, S. D.; Fabris, M.; Ferrari, V.; Carbonare, M. D.; Leon, A. *Free Radical Biol. Med.* **1997**, *22*, 669. (b) Moosmann, B.; Behl, C. *Proc. Natl. Acad. Sci. U.S.A.* **1999**, *96*, 8867.

(5) The Parkinson Study Group *N. Engl. J. Med.* **1993**, *328*, 176.

(6) Greenspan, H. C.; Aruoma, O. I. *Immunol. Today* **1994**, *15*, 209.

(7) (a) Bors, W.; Michel, C.; Saran, M. *Methods Enzymol.* **1994**, *234*, 420. (b) Jovanovic, S. V.; Steenken, S.; Tosic, M.; Marjanovic, B.; Simic, M. G. *J. Am. Chem. Soc.* **1994**, *116*, 4846.

(8) Decharneux, T.; Dubois, F.; Beauloye, C.; Wattiaux-De Coninck, S.; Wattiaux, R. *Biochem. Pharmacol.* **1992**, *44*, 1243.

(9) Torel, J.; Cillard, J.; Cillard, P. *Phytochemistry* **1986**, *25*, 383.

(10) (a) Guo, Q.; Zhao, B.; Shen, S.; Hou, J.; Hu, J.; Bors, W.; Michel, C.; Stettmaier, K. *Arch. Biochem. Biophys.* **2000**, *374*, 347. (b) Dangles, O.; Fargeix, G.; Dufour, C. *J. Chem. Soc., Perkin Trans. 2* **2000**, 1653. (c) Valcic, S.; Burr, J. A.; Timmermann, B. N.; Liebler, D. *C. Chem. Res. Toxicol.* **2000**, *13*, 801.

(11) (a) Rice-Evans, C. A.; Miller, N. J.; Paganga, G. *Free Radical Med.* **1996**, *20*, 933. (b) van Acker, S. A. B. E.; Bast, A.; Van Der Vijgh, W. J. F. *Antioxidants Health Dis.* **1998**, 221.

(12) Van Acker, S. A. B. E.; de Groot, M. J.; van den Berg, D.J.; Tromp, M. N. J. L.; Doone-Op den Kelder, G.; van der Vijgh, W. J. F.; Bast, A. *Chem. Res. Toxicol.* **1996**, *9*, 1305.

(13) Guiso, M.; Marra, C.; Cavarischia, C. *Tetrahedron Lett.* **2001**, *42*, 6531.

(14) Goto, N.; Shimizu, K.; Komuro, E.; Tsuchiya, J.; Noguchi, N.; Niki, E. *Biochim. Biophys. Acta* **1992**, *1128*, 147.

(15) (a) Hiramoto, K.; Ojima, N.; Sako, K.; Kikugawa, K. *Biol. Pharm. Bull.* **1996**, *19*, 558−563. (b) Yamashita, N.; Tanemura, H.; Kawanishi, S. *Mutat. Res.* **1999**, *425*, 107. (c) Nakanishi, I.; Fukuhara, K.; Ohkubo, K.; Shimada, T.; Kansui, H.; Kurihara, M.; Urano, S.; Fukuzumi, S.; Miyata, N. *Chem. Lett.* **2001**, 1152.

JA0178259

ELSEVIER

Mutation Research 521 (2002) 29–35

MR
Genetic Toxicology and Environmental Mutagenesis

www.elsevier.com/locate/gentox
Community address: www.elsevier.com/locate/mutres

The 4′-hydroxy group is responsible for the in vitro cytogenetic activity of resveratrol

Atsuko Matsuoka [a,*], Kenji Takeshita [b], Ayumi Furuta [c], Masayasu Ozaki [d], Kiyoshi Fukuhara [e], Naoki Miyata [f]

[a] *Division of Medical Devices, National Institute of Health Sciences, 1-18-1 Kamiyoga, Setagaya-ku, Tokyo 158-8501, Japan*
[b] *Ube Scientific Analysis Laboratory Inc., Ube-shi, Yamaguchi 755-8633, Japan*
[c] *Environmental Biological Life Science Research Center Inc., 555 Ukawa, Minakuchi-cho, Koka-gun, Shiga, Japan*
[d] *Tobacco Science Research Center, Japan Tobacco Inc., 6-2 Umegaoka, Aoba-ku, Kanagawa, Yokohama-city, Kanagawa 227-8512, Japan*
[e] *Division of Organic Chemistry, National Institute of Health Sciences, 1-18-1 Kamiyoga, Setagaya-ku, Tokyo 158-8501, Japan*
[f] *Department of Organic and Medicinal Chemistry, Graduate School of Pharmaceutical Sciences, Nagoya City University, 3-1 Tanabe-dori, Mizuho-ku, Nagoya 467-8603, Japan*

Received 19 April 2002; received in revised form 30 July 2002; accepted 30 July 2002

Abstract

We previously reported that 3,5,4′-trihydroxy-*trans*-stilbene (resveratrol), a polyphenolic phytoalexin found in grapes, induces a high frequency of sister chromatid exchanges (SCEs) in vitro. In this study, to investigate structure activity relationships, we synthesized six analogues of resveratrol differing in number and position of hydroxy groups, and we investigated their activity in chromosomal aberration (CA), micronucleus (MN) and sister chromatid exchange (SCE) tests in a Chinese hamster cell line (CHL). Two of the six analogues (3,4′-dihydroxy-*trans*-stilbene and 4-hydroxy-*trans*-stilbene) showed clear positive responses in a concentration-dependent manner in all three tests. Both were equal to or stronger than resveratrol in genotoxicity. The 4′-hydroxy (OH) analogue had the simplest chemical structure and was the most genotoxic. The other analogues did not have a 4′-hydroxy group. These results suggested that a 4′-hydroxy group is essential to the genotoxicity of stilbenes.

Keywords: Resveratrol; The 4′-hydroxy group; Stilbene; Sister chromatid exchanges (SCEs); Chromosome aberrations; Micronuclei

1. Introduction

3,5,4′-Trihydroxy-*trans*-stilbene (resveratrol) is a polyphenolic phytoalexin found in grapes, peanuts, the Japanese traditional medicine Kojokon, and in other foods. Resveratrol acts as an antioxidant, modulates lipid and lipoprotein metabolism, inhibits platelet aggregation, and has anti-inflammatory, anti-cancer, and estrogenic activity [1]. Resveratrol may play a role in the inverse correlation between red wine consumption and incidence of cardiovascular disease reported in epidemiological studies (the French paradox). Resveratrol has a similar chemical structure to diethylstilbestrol (DES), which induces numerical chromosome aberrations in vitro [2,3].

We previously reported [4] that resveratrol is negative in the bacterial reverse mutation assay but induces micronuclei (MN) and sister chromatid exchanges (SCEs) in vitro. Having got these results, we became interested in the role of the hydroxy groups on the

* Corresponding author. Tel.: +81-3-3700-9264; fax: +81-3-3707-6950.
E-mail address: matsuoka@nihs.go.jp (A. Matsuoka).

1383-5718/02/$ – see front matter
PII: S1383-5718(02)00211-5

genotoxic activity. We synthesized six analogues of resveratrol and compared their genotoxic activity with that of resveratrol.

2. Materials and methods

2.1. Cells

The Chinese hamster lung fibroblast cell line (CHL) [5] was maintained in Eagle's minimum essential medium (MEM; GIBCO 61100-061) supplemented with 10% heat-inactivated calf serum (Cansera International Inc., Rexdale, Ont., Canada). The doubling time was around 13 h and the modal chromosome number was 25.

2.2. Chemicals

The chemical structures of 3,5,4′-trihydroxy-*trans*-stilbene (resveratrol; CAS No. 501-36-0) and its six analogues are shown in Fig. 1. Resveratrol was purchased from Sigma (St. Louis, MO, USA). The analogues, 3,5,3′-trihydroxy-*trans*-stilbene (Fig. 1a); 3,5-dihydroxy-*trans*-stilbene (Fig. 1b); 3,4′-dihydroxy-*trans*-stilbene (Fig. 1c); 3,3′-dihydroxy-*trans*-stilbene (Fig. 1d); 3-hydroxy-*trans*-stilbene (Fig. 1e); and 4-hydroxy-*trans*-stilbene (Fig. 1f) were synthesized as previously reported [6]. All the chemicals were dissolved in physiological saline for use.

2.3. Genotoxicity tests

In all experiments we used 10 μg/ml of resveratrol in 48-h treatments as a concurrent positive control and showed the data at the right end of each graph. So we could compare these data with our previous data for resveratrol, and because the molecular weights of resveratrol and its analogues were similar, we used the same concentrations (2.5, 5, 10, and 20 μg/ml) of all the chemicals in all the studies.

2.3.1. Chromosomal aberration (CA) test

Cells were seeded at 1.5×10^5 per plate (60 mm in diameter). After 17-h incubation, they were treated with a test chemical for 24 or 48 h. Colcemid

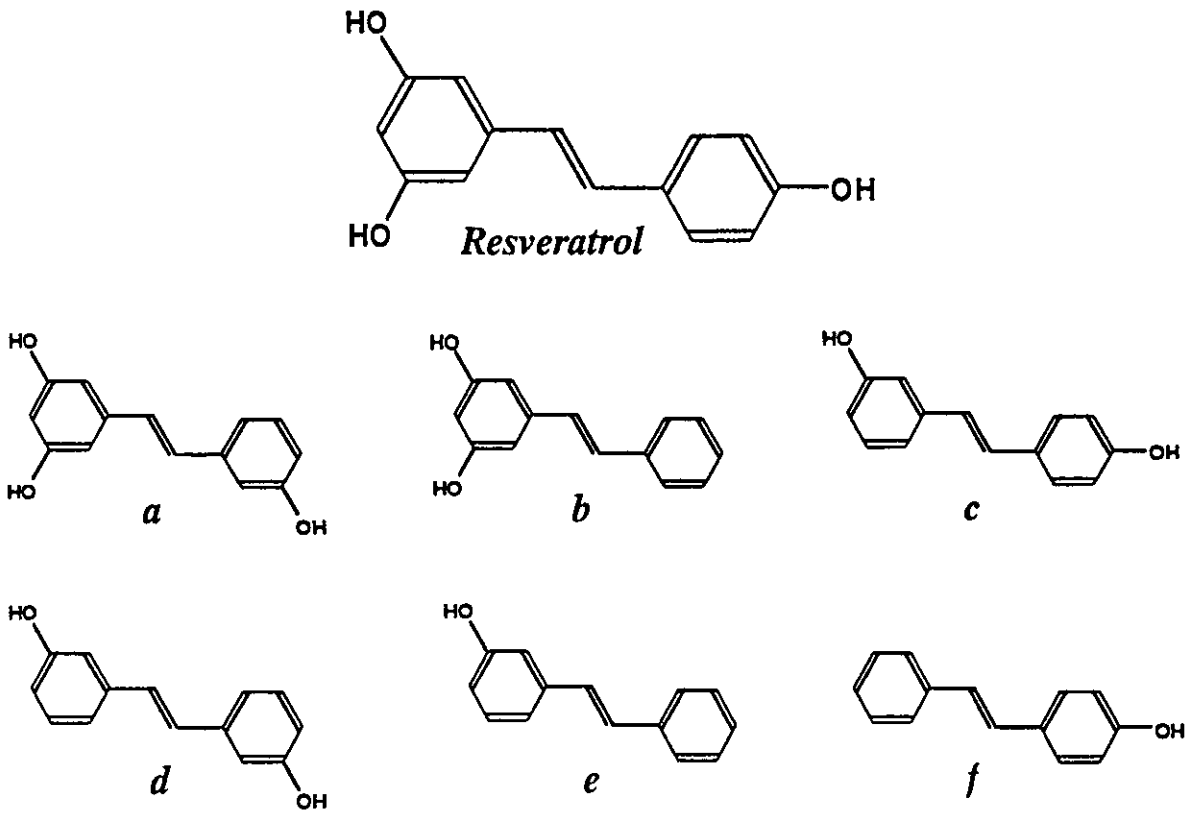

Fig. 1. Chemical structures of resveratrol and its synthesized analogues.

(0.2 μg/ml) was added for the final 2 h. Chromosome preparations were made as previously reported [7] and then stained with Giemsa solution. All slides were coded and the number of cells with numerical and structural aberrations was analyzed for 100 well-spread metaphase cells per concentration. The treatments were judged as negative (−) if the total aberration frequency was <5.0%, suspect (±) if 5.0 to <10.0%, and positive (+) if 10.0% or more, based on our historical database [7]. Solvent-treated cells served as the negative control. The CA tests were performed twice.

2.3.2. Micronucleus (MN) test

The MN test was performed twice, in parallel with the CA test. Cells were seeded and treated as they were in the CA test. MN preparations were made as previously reported [8]. The cells were stained by mounting in 40 μg/ml acridine orange in Ca^{2+}–Mg^{2+}-free phosphate-buffered saline and immediately observed at 400× magnification by fluorescence microscopy with a model Olympus BX50 and a U-MWB filter.

All slides were coded and the number of micronucleated cells among 1000 intact interphase cells was scored. In addition, we examined 1000 total cells and scored polynuclear and karyorrhectic (PN) cells and mitotic (M) cells as previously reported [9]. We analyzed the data using a χ^2-test for treated versus control groups. PN and M cell frequencies >100 and 50, respectively, were considered biologically significant.

2.3.3. Sister chromatid exchange (SCE) test

The SCE test was performed in parallel with the CA and MN test. Cells were seeded and treated as they were in the CA test. 5-Bromodeoxyuridine was added to the plate to a final concentration of 5 μM just after addition of the test chemical. Chromosome preparations were made as they were in the CA test. A fluorescence-plus-Giemsa technique [10] was used for sister chromatid differentiation staining as previously reported [11]. SCEs were scored on 25 second-metaphase (M2) cells that had 25 chromosomes and no CAs. Centromeric SCEs were indistinguishable from centric twists and were not scored. Solvent-treated cells served as the negative control. SCE data were analyzed with the Mann–Whitney *U*-test (the normal, two-tailed version).

3. Results

The results of the CA test are shown in Fig. 2. Significant polyploidy induction was not observed with any analogues (data not shown). Analogues c and f clearly induced structural chromosome aberrations, with peak frequencies of 63% at 10 μg/ml and 65% at 20 μg/ml, respectively. Chromatid breaks and exchanges were the main aberrations for both analogues. Analogue b induced severe cytotoxicity at 20 μg/ml in both the 24- and 48-h treatments. We observed no metaphases when analogue c was administered at 10 or 20 μg/ml for 24 h or 20 μg/ml for 48 h, or when analogue f was administered at 20 μg/ml for 48 h. The frequencies of CAs in cells treated with resveratrol were within expected values.

The results of the MN test are shown in Fig. 3. Reduction of M cell frequency, as shown for analogue c, is a rough indicator of cytotoxicity. Cell number counts performed in parallel showed a similar tendency as the M cell frequency (data not shown).

Analogue c induced a statistically significant increase in MN and PN cell frequency in 48-h treatments at low concentrations, but the frequencies decreased at higher concentrations due to the inhibition of cell division, as shown by the M cell data. Analogue f clearly induced MN and PN cells in a concentration-dependent manner, inducing at the same time, interestingly, gourd-shaped karyorrhectic cells.

The results of the SCE test are shown in Fig. 4. The frequency of SCE in a treatment time with the higher ratio of M2 cells to total cells is represented. Only analogues c and f induced a significant increase in the frequency of SCE with clear concentration response relationships. We observed no metaphases following the administration of analogue c at 10 and 20 μg/ml and analogue f at 20 μg/ml.

4. Discussion

Of the six resveratrol analogues, only analogues c and f were clearly positive in all the cytogenetic studies performed, suggesting that a 4′-hydroxy (OH) group may play a major genotoxic role. Analogues c–e have a three OH group in common, and either another OH at the 4′ or 3′ position or no other OH group. Among those only analogue c induced a strong

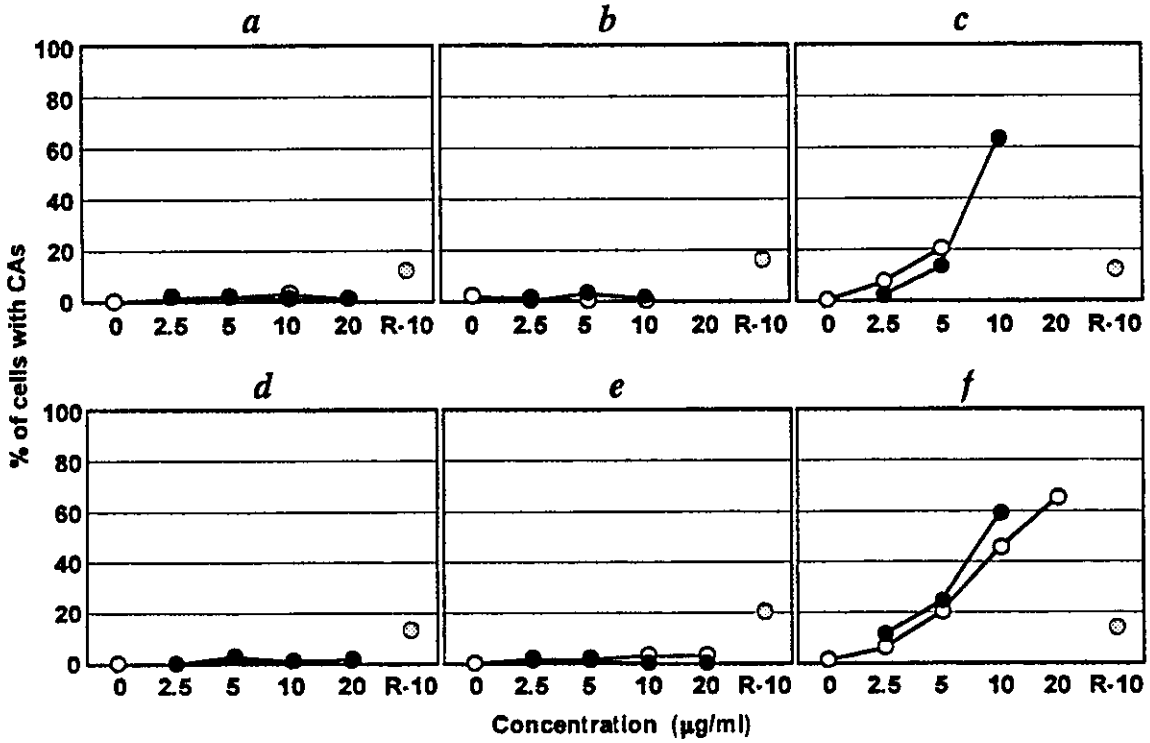

Fig. 2. Chromosome aberrations induced in vitro by resveratrol at 10 μg/ml (R-10) and its analogues. CHL cells were treated for 24 h (○) or 48 h (●).

response, further suggesting the strong contribution of the 4′-OH group. Finally analogue f, which has an OH group only at the 4′ position, induced a strong response, indicating directly the genotoxic role of the 4′-OH group.

Although analogues c and f both induced a high frequency of SCEs, analogue f induced a high frequency of PN cells, especially gourd-shaped karyorrhectic cells. That was accompanied by M cell reduction, suggesting induction of a kind of differentiation. It is not clear at present whether these cells remain blocked for a long time or die off.

Two other stilbenes with a 4′-OH group also exert biological activities. One is DES, which is a synthetic estrogen and induces polyploidy at low doses in CHL cells [2,3] and shows a high binding affinity for human ERα and ERβ [12]. The other is tamoxifen, an antiestrogen used to treat breast cancer. The 4-OH metabolite of tamoxifen is a potent antiestrogen [13,14].

Fukuhara et al. [15] reported that resveratrol is a Cu^{2+}-dependent DNA damaging agent whose activity is likely to be due to a copper-peroxide complex. They suggested the binding ability of resveratrol with Cu^{2+} was advantageous to induce Cu^{2+}-dependent DNA scission. Ahmad et al. also pointed out the significance of DNA damage induced by resveratrol—Cu^{2+} system, which is biologically active as assayed by bacteriophage inactivation [16]. Binding of resveratrol with Cu^{2+} is proved by monitoring the UV absorption spectra, which shows that the absorbance of resveratrol at 305 nm decreases with the concentration of Cu^{2+} [17]. In fact, the same spectral change was observed by analogues c and f whereas the addition of Cu^{2+} did not affect the spectra of the other analogues (data not shown), suggesting the specific binding of Cu^{2+} at the 4′-OH group of stilbene.

We reported that resveratrol shows potent cytogenetic activities previously [4]. In the present study, analogues c and f, which have a OH group at the 4′ position that may be responsible for cytogenetic activity of resveratrol, showed strong cytogenetic activities in a concentration-dependent manner in all three tests. In general, genotoxicity tests (the bacterial reverse mutation assay, the CA test, the MN test and so on) have been used to detect gene mutation, chromosome aberration, and DNA damage induced by physical and chemical agents. A positive result in genotoxicity tests has been considered "unbeneficial" to human.

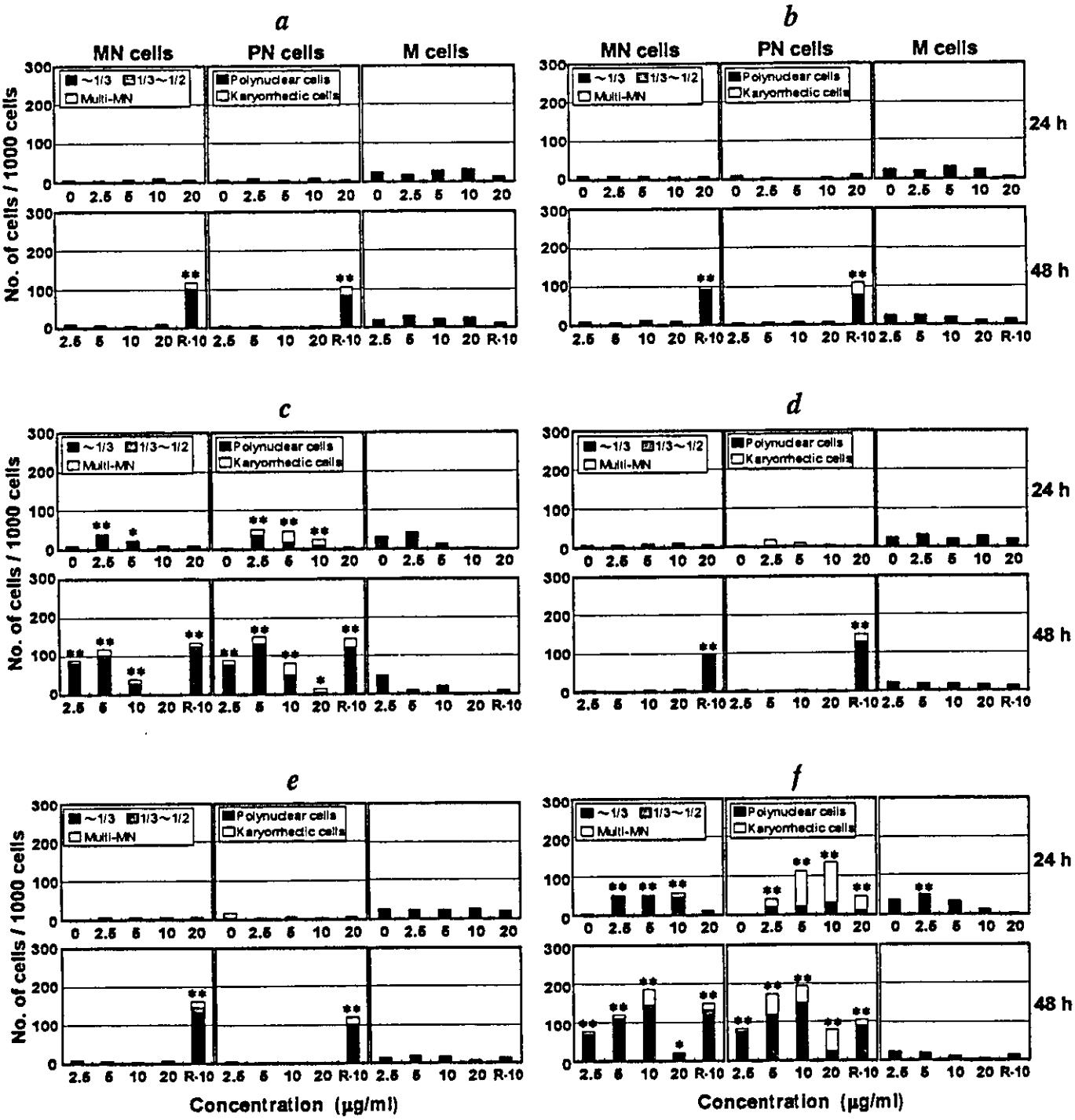

Fig. 3. Micronuclei induced in vitro by resveratrol at 10 μg/ml (R-10) and its analogues: (left) number of MN per 1000 intact interphase cells, black portion: cells with MN whose diameter is less than one-third of the main nucleus diameter, shadowed portion: cells with a MN whose diameter is one-third to one half the diameter of the main nucleus, white portion: cells with multiple MN; (middle) number of PN per 1000 total cells including karyorrhectic cells: black portion: polynuclear cells, white portion: karyorrhectic cells; (right) number of M per 1000 total cells. $^{*}P < 0.05$, $^{**}P < 0.01$.

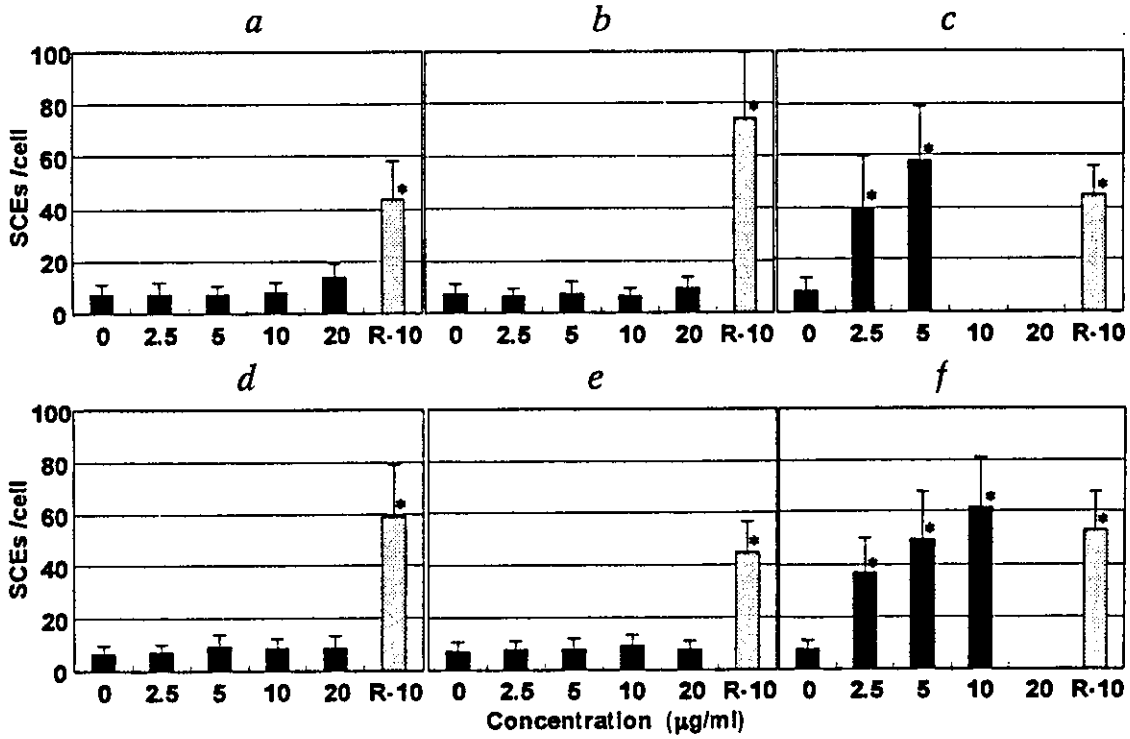

Fig. 4. SCE induced in vitro by resveratrol at 10 μg/ml (R-10) and its analogues. The values indicate the average SCEs per cell of 25 M2 cells and bars indicate S.D. $^{*}P < 0.001$.

Resveratrol, however, has been reported to show many beneficial effects in pharmacological aspects [1]. Does a negative result in genotoxicity tests mean that the test material is safe and beneficial to human? We think that a negative result might be due to not having any biological activities in a way. We think that a genotoxicity-positive chemical might not always be unbeneficial to human, as shown by resveratrol.

In conclusion, resveratrol, which has a variety of pharmacological activities, induced a high frequency of SCEs. Resveratrol analogues having a 4′-OH group also induced a high frequency of SCE and might also have similar pharmacological effects. Further studies are needed to test that and the role of the 4′-OH group in those effects.

References

[1] L. Fremont, Minireview: biological effects of resveratrol, Life Sci. 66 (2000) 663–673.
[2] M. Sawada, M. Ishidate Jr, Colchicine-like effect of diethylstilbestrol (DES) on mammalian cells in vitro, Mutat. Res. 57 (1978) 175–182.
[3] T. Sofuni (Ed.), Data Book of Chromosomal Aberration Test in Vitro, revised edition 1998, LIC, Tokyo, 1999, p. 184.
[4] A. Matsuoka, A. Furuta, M. Ozaki, K. Fukuhara, N. Miyata, Resveratrol, a naturally occurring polyphenol, induces sister chromatid exchanges in a Chinese hamster lung (CHL) cell line, Mutat. Res. 494 (2001) 107–113.
[5] M. Ishidate Jr, S. Odashima, Chromosome tests with 134 compounds on Chinese hamster cells in vitro—a screening for chemical carcinogens, Mutat. Res. 48 (1977) 337–354.
[6] K. Thakkar, R.L. Geahlen, M. Cushman, Synthesis and protein-tyrosine kinase inhibitory activity of polyhydroxylated stilbene analogues of piceatannol, J. Med. Chem. 36 (1993) 2950–2955.
[7] A. Matsuoka, T. Sofuni, N. Miyata, M. Ishidate Jr, Clastogenicity of 1-nitropyrene, dinitropyrenes, fluorene and mononitrofluorenes in cultured Chinese hamster cells, Mutat. Res. 259 (1991) 103–110.
[8] A. Matsuoka, N. Yamazaki, T. Suzuki, M. Hayashi, T. Sofuni, Evaluation of the micronucleus test using a Chinese hamster cell line as an alternative to the conventional in vitro chromosomal aberration test, Mutat. Res. 272 (1993) 223–236.
[9] A. Matsuoka, K. Matsuura, H. Sakamoto, M. Hayashi, T. Sofuni, A proposal for a simple way to distinguish aneugens from clastogens in the in vitro micronucleus test, Mutagenesis 14 (1999) 385–389.
[10] P. Perry, S. Wolff, New Giemsa method for the differential staining of sister chromatids, Nature 251 (1974) 156–158.
[11] A. Matsuoka, M. Ozaki, K. Takeshita, H. Sakamoto, H.-R. Glatt, M. Hayashi, T. Sofuni, Aneuploidy

induction by benzo[a]pyrene and polyploidy induction by 7,12-dimethylbenz[a]anthracene in Chinese hamster cell lines V79-MZ and V79, Mutagenesis 12 (1997) 365–372.
[12] G.N. Nikov, M. Eshete, R.V. Rajnarayanan, W.L. Alworth, Interactions of synthetic estrogens with human estrogen receptors, J. Endocrinol. 170 (2001) 137–145.
[13] V.C. Jordan, M.M. Collins, L. Rowsby, G. Prestwich, A monohydroxylated metabolite of tamoxifen with potent antiestrogenic activity, J. Endocrinol. 75 (1977) 305–316.
[14] V.C. Jordan, M.E. Lieberman, E. Cormier, R. Koch, J.R. Bagley, P.C. Ruenitz, Structural requirements for the pharmacological activity of nonsteroidal antiestrogens in vitro, Mol. Pharmacol. 26 (1984) 272–278.
[15] K. Fukuhara, N. Miyata, Resveratrol as a new type of DNA-cleaving agent, Bioorg. Med. Chem. Lett. 8 (1998) 3187–3192.
[16] A. Ahmad, S.F. Asad, S. Singh, S.M. Hadi, DNA breakage by resveratrol and Cu(II): reaction mechanism and bacteriophage inactivation, Cancer Lett. 154 (2000) 29–37.
[17] L. Belguendouz, L. Fremont, A. Linard, Resveratrol inhibits metal ion-dependent and independent peroxidation of porcine low-density lipoproteins, Biochem. Pharmacol. 53 (1997) 1347–1355.

ELSEVIER

Mutation Research 521 (2002) 187–200

MR
Genetic Toxicology and Environmental Mutagenesis

www.elsevier.com/locate/gentox
Community address: www.elsevier.com/locate/mutres

Effect of 10-aza-substitution on benzo[*a*]pyrene mutagenicity in vivo and in vitro

Katsuya Yamada[a], Takayoshi Suzuki[b], Arihiro Kohara[a,b], Makoto Hayashi[b], Atsushi Hakura[c], Takaharu Mizutani[a], Ken-ichi Saeki[a,*]

[a] *Faculty of Graduate School of Pharmaceutical Sciences, Nagoya City University, Tanabedori, Mizuho-ku, Nagoya 467-8603, Japan*
[b] *Division of Genetics and Mutagenesis, National Institute of Health Sciences, 1-18-1 Kamiyoga, Setagaya-ku, Tokyo 158-8501, Japan*
[c] *Drug Safety Research Laboratories, Eisai Co. Ltd., 1 Takehaya-machi, Kawashima-cho, Hashima-gun, Gifu 501-6195, Japan*

Received 28 June 2002; received in revised form 10 September 2002; accepted 10 September 2002

Abstract

Benzo[*a*]pyrene (BaP), an environmental carcinogen, shows genotoxicity after metabolic transformation into the bay-region diol epoxide, BaP-7,8-diol 9,10-epoxide. 10-Azabenzo[*a*]pyrene (10-azaBaP), in which a ring nitrogen is located in the bay-region, is also a carcinogen and shows mutagenicity in the Ames test in the presence of the rat liver microsomal enzymes. In order to evaluate the effect of aza-substitution on in vivo genotoxicity, BaP and 10-azaBaP were assayed for their in vivo mutagenicity using the *lacZ*-transgenic mouse (Muta^{TM}Mouse). BaP was potently mutagenic in all of the organs examined (liver, lung, kidney, spleen, forestomach, stomach, colon, and bone marrow), as described in our previous report, whereas, 10-azaBaP was slightly mutagenic only in the liver and colon. The in vitro mutagenicities of BaP and 10-azaBaP were evaluated by the Ames test using liver homogenates prepared from several sources, i.e. CYP1A-inducer-treated rats, CYP1A-inducer-treated and non-treated mice, and humans. BaP showed greater mutagenicities than 10-azaBaP in the presence of a liver homogenate prepared from CYP1A-inducer-treated rodents. However, 10-azaBaP showed mutagenicities similar to or more potent than BaP in the presence of a liver homogenate or S9 from non-treated mice and humans. These results indicate that 10-aza-substitution markedly modifies the nature of mutagenicity of benzo[*a*]pyrene in both in vivo and in vitro mutagenesis assays.

Keywords: Aza-substitution; In vivo mutagenesis assay; Mutation spectrum; Human liver microsome

1. Introduction

Benzo[*a*]pyrene (BaP) is one of the most ubiquitous environmental contaminants and has potent carcinogenicity and mutagenicity [1–3]. BaP is converted to the bay-region diol epoxide, which is the ultimate activated form [4,5]. The bay-region theory applies as a common mechanism to other polycyclic aromatic hydrocarbons. In addition, BaP has an ability to induce cytochrome P4501A1 (CYP1A1), which is involved in the metabolic activation of BaP itself [6–9].

10-Azabenzo[*a*]pyrene (10-azaBaP), a BaP analog containing a nitrogen atom at position-10, is also an environmental contaminant [10]. Kosuge et al. obtained 7.3 mg of 10-azaBaP from 82 g of a basic fraction of coal tar [10]. This amount of 10-azaBaP indicates that its environmental content of 10-azaBaP might be much lower than that of BaP. 10-AzaBaP

* Corresponding author. Tel.: +81-52-836-3485; fax: +81-52-834-9309.
E-mail address: saeki@phar.nagoya-cu.ac.jp (K.-i. Saeki).

1383-5718/02/$ – see front matter © 2002 Elsevier Science B.V. All rights reserved.
PII: S1383-5718(02)00240-1

was reported to be carcinogenic [11] and to have as much mutagenicity as BaP in the Ames test using *Salmonella typhimurium* TA100 in the presence of the rat liver S9 mix, although formation of the bay-region diol epoxide of 10-azaBaP seems impossible because of the nitrogen atom at position-10 [12–14]. Therefore, 10-azaBaP might be converted to an ultimate form not by the bay-region mechanism but by other unknown mechanisms.

In this report, we undertook to evaluate the effect of ring 10-aza-substitution of BaP on its in vivo mutagenicity in an assay system using the *lacZ*-transgenic mouse (Muta^{TM}Mouse) [15]. In addition, we assessed the in vitro mutagenicities of BaP and 10-azaBaP by Ames test. In these assays, we used liver homogenates prepared from several sources, i.e. CYP1A-inducer-treated rats, CYP1A-inducer-treated and non-treated mice, and humans, to investigate species differences of the metabolic activation enzymes responsible for the in vitro mutagenicity of BaP and 10-azaBaP.

2. Materials and methods

2.1. Materials

BaP (CAS Registry no. 50-32-8) and phenyl-β-D-galactoside (P-gal) were purchased from Sigma, Cofactor I^{TM} from Oriental Yeast Co. (Tokyo), proteinase K and olive oil from Wako Pure Chemicals (Osaka), RNase from Boeringer Mannheim, 3-methylcholanthrene (CAS Registry no. 56-49-5) from Aldrich, and pooled human liver S9 (20 mg protein/ml) from Gentest Co. (Woburn, MA, USA). 10-AzaBaP (CAS Registry no. 189-92-4) was synthesized according to the reported methods [16]. Purification of the product by re-crystallization from acetone yielded 10-azaBaP as pale brown needles: m.p. 158–161 °C. Anal. Calcd. for $C_{19}H_{11}N$: C, 90.09; H, 4.38; N, 5.53. Found: C, 89.86; H, 4.60; N, 5.40.

2.2. In vivo mutagenesis assay using Muta^{TM}Mouse

2.2.1. Animals and treatments

Male Muta^{TM}Mice, at 7–8 weeks of age, were supplied by COVANCE Research Products (PA, USA) and acclimatized for 1 week before use. The test chemicals dissolved in olive oil (12.5 ml/kg body weight) were administered to five mice at a daily dose of 125 mg/kg for five consecutive days by gavage. Five control mice were given olive oil.

2.2.2. Tissue and DNA isolation

All mice were killed by cervical dislocation 14 days after the last administration of test chemicals. The liver, spleen, kidney, lung, colon, stomach, forestomach, and bone marrow were immediately extirpated, frozen in liquid nitrogen, and stored at −80 °C until DNA extraction. The genomic DNA was extracted from each tissue by the phenol/chloroform method as previously reported [17]. The isolated DNA, which was precipitated with ethanol, was air-dried and dissolved in an appropriate volume (20–200 μl) of TE-4 buffer (10 mM Tris–HCl at pH 8.0 containing 4 mM EDTA) at room temperature overnight. The DNA solution thus prepared was stored at 4 °C.

2.2.3. In vitro packaging

The λgt10/*lacZ* vector could be efficiently recovered by in vitro packaging reactions [18]. Our homemade packaging extract (HM) consisting of sonic extract (SE) of *Escherichia coli* NM759 and freeze–thaw lysate (FTL) of *E. coli* BHB2688 was prepared according to the method of Gunther et al. [19]. As a general procedure for handling the HM extract, approximately 5 μg DNA was mixed with 15 μl of FTL and 30 μl of SE and incubated at 37 °C for 90 min. Then SE and FTL were added again and the mixture was incubated for another 90 min. The reaction was terminated by the addition of an appropriate volume of SM buffer (50 mM Tris–HCl at pH 7.5, 10 mM $MgSO_4$, 100 mM NaCl, 0.01% gelatin) and the mixture was stored at 4 °C. By this procedure, the λgt10 vector to form an infectious phage was efficiently rescued from genomic DNA.

2.2.4. Mutation assay

2.2.4.1. lacZ mutant frequency determination. The positive selection for *lacZ* mutants was performed as previously reported [17,20]. Briefly, the phage solution was absorbed to *E. coli* C (*lac*$^{-}$ *galE*$^{-}$) at room temperature for 20–30 min. For titration, appropriately diluted phage–*E. coli* solution was mixed with LB top agar (containing 10 mM $MgSO_4$) and plated

onto dishes containing bottom agar. The remaining phage–*E. coli* solution was mixed with LB top agar containing P-gal (3 mg/ml) and plated as described above. The mutant frequency (MF) was calculated by the following formula:

$$\text{mutant frequency} = \frac{\text{total number of plaques on selection plates}}{\text{total number of plaques on titer plates}} \times \text{dilution factor.}$$

The significance of differences in the mutant frequency between the treated and control groups was analyzed by using Student's *t*-test.

2.2.4.2. cII mutant frequency determination. In the present study, we examined the mutagenicity in the λ *cII* gene, which is also integrated as a λ vector gene, which serves as another selective marker as reported previously in the *lacI* transgenic BigBlue mouse [21]. The positive selection for *cII* mutants was performed according to the method of Jakubczac et al. [21] with a slight modification as previously reported [22]. Briefly, the phage solution was absorbed to *E. coli* G1225 (*hfl*$^-$) at room temperature for 20–30 min. For titration, appropriately diluted phage–*E. coli* solution was mixed with LB top agar (containing 10 mM $MgSO_4$) and plated onto dishes containing bottom agar and the plates were incubated at 37 °C for 24 h. The remaining phage–*E. coli* solution was mixed with LB top agar and plated onto dishes containing bottom agar. The plates were incubated at 25 °C for 48 h for selection of *cII* mutants. The wild type phage, recovered from Muta^{TM}Mice, has a *cI*$^-$ phenotype, which permits plaque formation with the *hfl*$^-$ strain at 37 °C but not at 25 °C. The mutant frequency was calculated by the following formula:

$$\text{mutant frequency} = \frac{\text{total number of plaques on selection plates}}{\text{total number of plaques on titer plates}} \times \text{dilution factor.}$$

The significance of differences in the mutant frequency between the treated and control groups was analyzed by using Student's *t*-test.

2.2.5. Sequencing of mutants

The entire λ *cII* region was amplified directly from mutant plaques by *Taq* DNA polymerase (Takara Shuzo, Tokyo, Japan) with primers P1; 5′-AAAAAG-GGCATCAAATTAAACC-3′, and P2; 5′-CCGAAGT-TGAGTATTTTTGCTGT-3′ as previously reported [22,23] (Fig. 1). A 446 bp PCR product was purified with a microspin column (Amersham Pharmacia, Tokyo, Japan) and then used for a sequencing reaction with the Ampli *Taq* cycle sequencing kit (PE Biosystems, Tokyo, Japan) using the primer P1. The reaction product was isolated by ethanol precipitation and analyzed with the ABI PRISM^{TM} 310 genetic analyzer (PE Biosystems).

2.3. In vitro mutation assays (Ames test)

2.3.1. Preparation of the microsomal fraction of mice and rats

BaP dissolved in olive oil (100 mg/kg body weight) was injected intraperitoneally into 6 male 7–8-week-old CDF1 mice, the non-transgenic parent strain of Muta^{TM}Mouse. Only olive oil was injected into the other six mice as control. Twenty-four hours after the treatment, the mice were sacrificed by cervical dislocation and the livers were removed. The livers were then homogenized in 0.5 M potassium phosphate buffer (pH 7.4) (3 ml/g of liver).

3-Methylcholanthrene (3-MC)-induced rat liver microsomes were prepared according to the previous report [24]. Briefly, male Sprague–Dawley rats (6-week old) were intraperitoneally injected with 3-MC dissolved in corn oil at a daily dose of 50 mg/kg body weight for three consecutive days. The rats were fasted for 18 h and sacrificed by decapitation 48 h after the last 3-MC injection. The liver was rapidly excised and homogenized in 0.15 M KCl (3 ml/g liver).

The microsomal fraction was prepared by centrifuging the liver homogenate at 9000 × *g* for 20 min, centrifuging the resulting supernatant at 105,000 × *g* for 50 min, and re-suspending the 105,000 × *g* pellet in 0.5 M potassium phosphate buffer (pH 7.4). The microsomal protein contents measured by the Bradford method [25] were as follows; BaP-treated mouse microsomes, 16.2 mg/ml; non-treated mouse microsomes, 17.2 mg/ml; 3-MC-treated rat microsomes, 9.3 mg/mL

2.3.2. Ames test

Chemicals were tested for mutagenicity as previously reported using *S. typhimurium* TA100 in the presence of the liver homogenate (S9 or microsomal

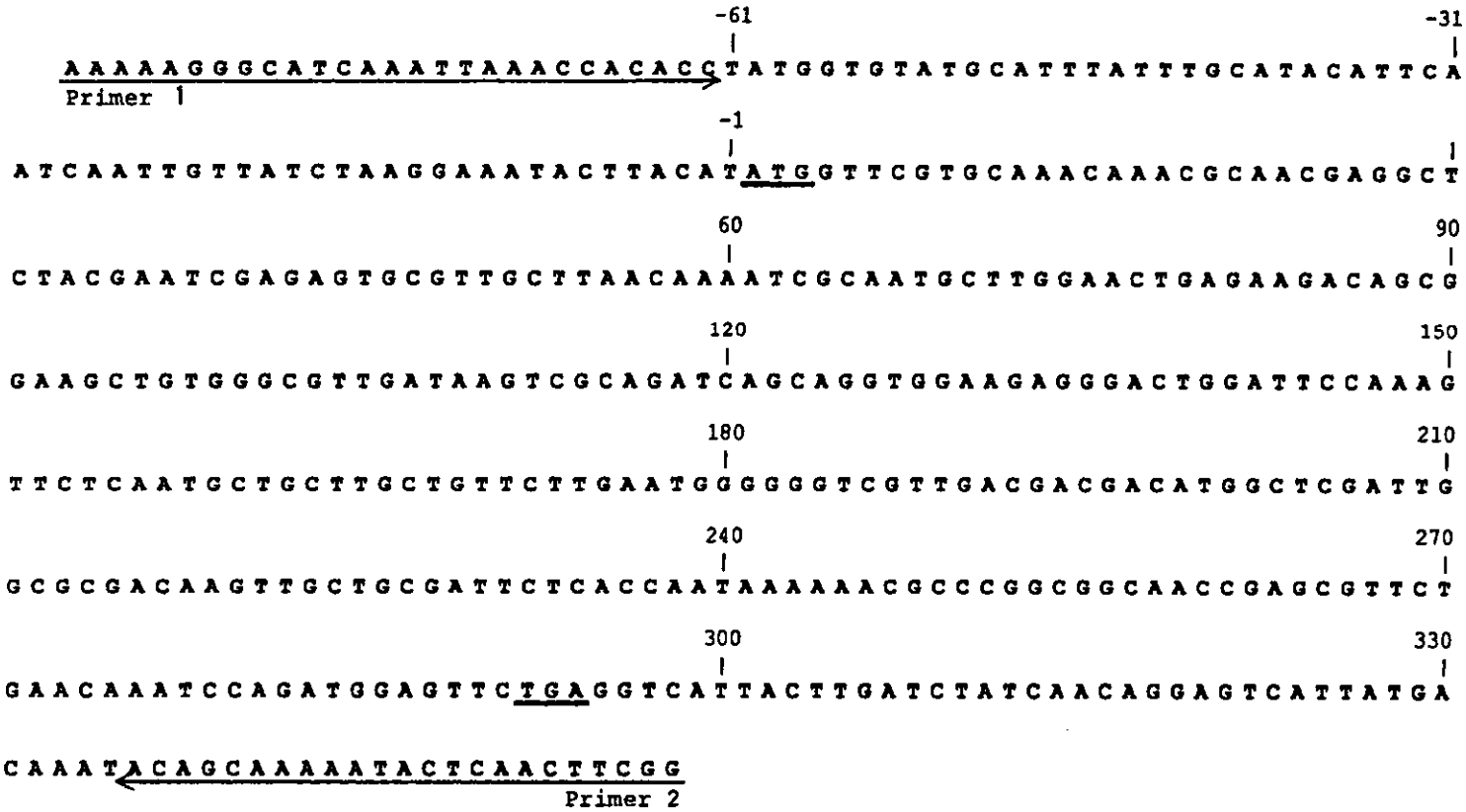

Fig. 1. Sequence map of the *cII* gene. Primers, used for PCR amplification and sequencing, are shown by arrows. The PCR gives 446 bp products that involve the entire (294 bp) *cII* gene. Initiation and stop codons are underlined.

fraction) and cofactors (Cofactor I™) [24,26]. Cofactor I™ consisted of 4 mM NADPH, 4 mM NADH, 5 mM glucose-6-phosphate, 32.8 mM KCl, 8 mM $MgCl_2$, and 100 mM phosphate buffer (pH 7.4). The TA100 strain was provided by Dr. B.N. Ames of the University of California, Berkeley. Assays were carried out by pre-incubation of the test chemical with the S9 or microsome mix at 37 °C for 20 min. At least three independent experiments were performed.

3. Results

3.1. In vivo mutagenicity of BaP and 10-azaBaP

3.1.1. Mutant frequency (MF)

BaP and its nitrogen-containing analog, 10-azaBaP (Fig. 2), were tested for in vivo mutagenicity using *lacZ*-transgenic mice (Muta™Mice) at a daily dose of 125 mg/kg for five consecutive days. The mutant frequencies observed in the DNA preparations extracted from the eight organs 14 days after the last injection are shown in Table 1. Over 100,000 titer plaques or over 10 mutant plaques were analyzed in most organs. For the forestomach, the mutant frequency of one animal in the control group was missing and the *lacZ* mutants of two animals in the 10-azaBaP-treated group were insufficient because the amount of isolated DNA was not enough to analyze. For the same reason, some of the mutant numbers in the bone marrow were insufficient.

The spontaneous mutant frequencies observed in the control group were similar among the eight organs in both *lacZ* and *cII* assays, in a rate range of 55×10^{-6} to 90×10^{-6} and 31×10^{-6} to 56×10^{-6}, respectively. These results were comparable to our previous studies [17,22].

The dose and administration protocol for the BaP-treated Muta™Mice using the *lacZ* assay were the same as in the previous work reported by one of the authors (A.H.) [2]. BaP significantly increased the mutant frequencies in all organs in the *lacZ* assay like in the previous work. The mutant frequencies in the *cII* assay showed a tendency similar to those in the *lacZ* assay. The mutant frequencies in the forestomach and colon were more than 10-fold higher than the spontaneous mutant frequencies in both *lacZ* and *cII* assays.

On the other hand, 10-azaBaP significantly increased the mutant frequency only in the liver and colon in the *lacZ* assay (2.5- and 1.7-fold increases, respectively). In the *cII* assay, 10-azaBaP significantly increased the mutant frequency in the liver as in the *lacZ* assay whereas the mutant frequency in the colon was only slightly, but not significantly, increased. The mutant frequencies observed in the other organs were the same as the spontaneous mutant frequencies in both assays. Consequently, 10-azaBaP seems to have much less mutagenicity than BaP in both assays.

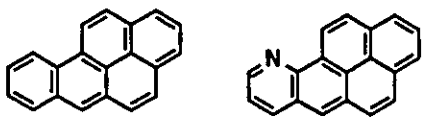

benzo[a]pyrene (BaP) 10-azabenzo[a]pyrene (10-azaBaP)

Fig. 2. Structures of BaP and 10-azaBaP.

3.1.2. Mutation spectra of BaP and 10-azaBaP

A total of 49 10-azaBaP-induced mutants were subjected to sequence analysis, together with 37 control mutants and 37 BaP-induced mutants. The mutations are characterized in Tables 2–4, and summarized in Table 5. In Table 5, the same mutations from an identical mouse were treated as a single event.

Spontaneous mutations consisted mainly of G:C to A:T transitions (18/32) followed by G:C to T:A transversions as shown in the previous report on the *cII* mutant spectrum in the control liver of Muta™Mouse [23].

The majority of BaP-induced mutations were G:C to T:A transversions (19/36), and the G:C to A:T transition had a low incidence (4/36) as in the previous report [3].

On the other hand, 10-azaBaP-induced mutations consisted mainly of base substitutions (38/44), G:C to A:T transitions (17/38) and G:C to T:A transversions (11/38) predominating. The 10-azaBaP-induced *cII* mutant spectrum, unlike with BaP, showed no characteristics compared with those in control mice.

3.2. In vitro mutagenicity of BaP and 10-azaBaP

In Muta™Mice, 10-azaBaP showed much less in vivo mutagenicity than BaP, though a previous report indicated that 10-azaBaP had as potent an in vitro mutagenicity as BaP in the Ames test using the